

High northern geomagnetic field behavior and new constraints on the Gilsá event: Paleomagnetic and $^{40}\text{Ar}/^{39}\text{Ar}$ results of $\sim 0.5\text{--}3.1$ Ma basalts from Jökuldalur, Iceland.

Arne Døssing^{a,b,*}, Adrian R. Muxworthy^b, Radchagrit Supakulopas^b,
Morten S. Riishuus^c, Conall Mac Niocaill^d

^a*Div. of Geomagnetism, DTU Space, Technical University of Denmark, Diplomvej, Building 371, 2800 Kgs. Lyngby, Denmark*

^b*Dept. of Earth Science and Engineering, Imperial College London, South Kensington Campus, London SW7 2AZ, UK*

^c*Nordic Volcanological Center, Institute of Earth Sciences, University of Iceland, Sturlugata 7, IS-101 Reykjavik*

^d*Dept. of Earth Sciences, University of Oxford, S Parks Rd, Oxford OX1 3AN, UK*

Abstract

Recent paleomagnetic results of extrusive rocks from high southern latitudes ($> 60^\circ\text{S}$) and high northern latitudes ($> 60^\circ\text{N}$) have been suggested to reflect a hemispheric asymmetry of the geomagnetic field on time-scales of 10^5 to 10^6 years, with higher and more stable fields in the north. This interpretation, however, is based on only a few modern-standard paleodirectional data sets and on high northern stable field paleointensity data of rocks that are mainly younger than 100 kyr. The sparsity of modern-standard data questions the validity (and age range) of this potential geomagnetic asymmetry. In 2013 and 2014, we sampled basaltic lava flows in Jökuldalur, north-eastern Iceland, to obtain high-standard paleodirectional and paleointensity data at relatively

*Corresponding author

Email address: ards@space.dtu.dk (Arne Døssing)

high-northern latitudes (65.2°N). On average, we sampled >15 cores per site at 51 sites of predominantly Matuyama age. Complete demagnetization was carried out on all samples using AF or thermal demagnetization. We present 45 distinct paleomagnetic directions based on overall $N > 10$ ChRMs per site and $\alpha_{95} < 3.5^\circ$. We obtain a mean direction of $D = 355.7^\circ$, $I = 76.3^\circ$, and $\alpha_{95} = 3.2$ for $N = 45$ sites that is not significantly different from a GAD field. The resulting 45 VGPs distribute around the North Pole, and the global mean paleomagnetic pole ($\bar{\lambda} = 87.8^\circ$, $\bar{\phi} = 224.3^\circ$) is coincident with the North Pole within the α_{95} confidence limit. We calculate a VGP dispersion for our 38 Matuyama age sites of $20.5^{23.3}_{17.8}$, which is $\sim 1\text{--}4^\circ$ lower than estimates from published Iceland data (from surveys that sampled 2–5 cores per site) but still supports the interpretation of a dependence of VGP dispersion on latitude during the Matuyama. Based on relatively strict cut-off criteria we also present six new field strength estimates from the time interval $\sim 1.2\text{--}1.83$ Ma, thus filling a large data gap of the high-northern stable field behaviour. We obtain a median VADM of 57 ± 3 ZAm² (VDM of 60 ± 5 Am²), which is higher than the median VADM of 16 intensity estimates from Antarctica (39 ± 7 ZAm²) from the same period. A higher northern field is also found when using less strict cut-off criteria resulting in 14 field estimates from Jökuldalur, i.e. we find support for higher field strength in the northern hemisphere as compared to the southern hemisphere during the Matuyama. Finally, we deliver a revised magneto-chronostratigraphic model of Jökuldalur and conduct an investigation of the type sections of the so-called Gilsá normal polarity event around 1.62 Ma. Our revised model is based on 11 new $^{40}\text{Ar}/^{39}\text{Ar}$ ages. No evidence is found of the existence of the

Gilsá event in Jökuldalur. Instead we find that the normal polarity intervals in the type sections can both be correlated to Olduvai subchron.

Keywords: Gilsá event, Paleosecular variation, Paleointensity, Matuyama, Iceland, Ar-Ar radiometric dating

1. Introduction

Satellite observations of the geomagnetic field show that it is dominated by a strong dipolar component, which is highly dynamic, changing chaotically in both direction and intensity. These temporal changes, known as geomagnetic secular variation, are thought to reflect both short- and long-term changes in fluid processes in the Earth's core (Johnson and McFadden, 2007). A fundamental assumption in our use of paleomagnetic data, e.g., in plate reconstruction studies is that when observed over geological timescales the secular variation is averaged out, and the time-averaged field (TAF) is a dipole field aligned with the rotation axis, the so called geocentric axial dipole field (GAD) (Hospers, 1954).

Recent paleomagnetic results from high latitudes ($>60^\circ$) have studied the apparent long-lived hemispheric asymmetry of the magnetic field on time-scales of 10^5 to 10^6 years, contrasting higher and more stable fields in the north with lower average strength and less stable fields in the south (Cromwell et al., 2015, 2013; Lawrence et al., 2009; Tauxe et al., 2004a). However, modern-standard high-latitude paleomagnetic data, especially absolute paleointensity data, of 0.1–5 Ma rocks are sparse (Figure 1a). Only sporadic temporal overlap exists between high-latitude northern and southern paleointensity data for rocks older than 100 kyr and, in particular, for

21 stable field periods (Figure 1b). Such data are vital in order to sample and
22 characterize high-latitude paleostructures of the radial magnetic field at the
23 Core-Mantle Boundary.

24 The basaltic lava sequences of Iceland (64–66°N) have been subject of
25 numerous paleomagnetic studies since the early 1950s, but with a majority
26 of studies focusing on stratigraphic mapping and/or extension of the ge-
27 omagnetic polarity time-scale, sampling 2–5 cores per site (e.g., Helgason
28 and Duncan, 2001; Kristjánsson et al., 1980, 2004; McDougall et al., 1977;
29 Udagawa et al., 1999; Watkins et al., 1975). Other studies have targeted
30 geomagnetic reversals (Camps et al., 2011) or excursions (Jicha et al., 2011;
31 Kristjánsson, 1999), or have focused on the field strength during transitional
32 events (Camps et al., 2011; Goguitchaichvili et al., 1999) or during the last
33 ~100 kyr (Cromwell et al., 2015; Tanaka et al., 2012). Little work has been
34 done on Icelandic rocks to produce modern-standard PSV and paleointensity
35 data for geomagnetic stable periods for rocks >100 kyr.

36 We present modern-standard paleomagnetic and $^{40}\text{Ar}/^{39}\text{Ar}$ radiometric
37 results of ~0.5–3.1 Ma rocks from Jökuldalur (Figure 1c), including absolute
38 paleointensity and PSV data. We provide stable field strength estimates for
39 the period 1–2 Ma, which allows us to carry out a comparison of high-latitude
40 northern and southern field behavior during this period (cf. Figure 1b). We
41 also present a revised magneto-chronostratigraphy of Jökuldalur, including
42 an examination of the Gilsá event, a short normal polarity subchron inferred
43 to exist around 1.62 Ma (McDougall and Wensink, 1966; Udagawa et al.,
44 1999).

2. Geology and paleomagnetic sampling

The first paleomagnetic studies in Jökuldalur (Figure 1c) were carried out by Wensink (1964a,b) who established the stratigraphy, covering the Brunhes to Gilbert epochs. The approximate time frame and the existence of the Matuyama reversed (R1) and Gauss normal (N2) polarity epochs was later supported by results of K-Ar radiometric dating (McDougall and Wensink, 1966; Watkins et al., 1975). Wensink (1964b) and McDougall and Wensink (1966) established the Olduvai normal subchron in Hnjúksá (HN) (Figure 1c) based on K-Ar dating. They further argued for a second normal polarity event at 1.60 ± 0.05 Ma (termed *Gilsá*) near the top of this section and above the Olduvai subchron. Subsequent resampling of section HN and additional K-Ar radiometric dating, however, indicated no evidence of this second event (Watkins et al., 1975).

In 1993, Udagawa et al. (1999) revisited Jökuldalur and collected samples from 38 lava flows, mainly from the younger part of the valley along Thverá (TH) and Krengilsá (KG) (Figure 1c). Based on paleomagnetic analysis and new K-Ar ages, Udagawa et al. (1999) correlated the lava flows to 0.5–1.8 Ma. They resurrected the idea of the normal Gilsá event around 1.61–1.62 Ma, this time in section KG. However, the reversely magnetized lavas, located stratigraphically below their inferred Gilsá event, were dated at 1.85 ± 0.08 Ma (2σ), i.e. probably within the Olduvai subchron (1.78–1.94 Ma) (cf. Gradstein et al., 2012): The existence of the Gilsá event is therefore debatable.

In 2013 and 2014, we resampled sections HN, KG and TH (Figures 1c and 2). In total, >700 cores were sampled at 51 sites (site average of ~ 15

70 cores). We sampled 42 sites in 2013 together with another 120 sites in
71 Fljótsdalur, east of Jökuldalur (work in progress). Based on stratigraphic
72 remapping of Jökuldalur in 2014, we sampled another three, previously un-
73 mapped, sites near the top of section TH (Figure 2: sites THA12, THA13
74 and THA15). Due to time constraints, we did not sample the few normal po-
75 larity sites of section HN near the river, below HN3. These sites are thought
76 to be of Gauss age (McDougall and Wensink, 1966).

77 Our sampling was mostly restricted to unaltered massive cores of basaltic
78 lavas in well-defined flow units (Figure 2). The sampling was generally car-
79 ried out over tens of meters to avoid the risk that samples were not *in situ*
80 or hit by lightning strikes. We oriented the samples mainly by using a sun
81 compass (71% of all samples). At sites sampled during cloud cover, we ori-
82 ented the samples by magnetic compass readings supplemented by bearings
83 to known landmarks. We used the bearings to correct our magnetic measure-
84 ments for these sites. Hand samples were collected from all sites to deliver
85 new $^{40}\text{Ar}/^{39}\text{Ar}$ radiometric age determinations.

86 3. Methodology

87 3.1. Sample preparation and $^{40}\text{Ar}/^{39}\text{Ar}$ dating method

88 We selected 11 basalt samples for new age determinations by the $^{40}\text{Ar}/^{39}\text{Ar}$
89 incremental heating method. The samples were selected based on their fi-
90 delity for Ar-Ar dating and the need for additional Ar-Ar dating in spe-
91 cific intervals. A detailed description of the sample preparation and dating
92 method is found in Section S1 (Suppl. Mat.).

93 3.2. Demagnetization experiment

94 Stepwise alternating-field (AF) and thermal demagnetization experiments
95 were initially conducted on two specimens per site to test the behavior of the
96 rocks to magnetic cleaning. For the AF demagnetization we used a Mol-
97 spin Tumbling AF Demagnetizer and a DETECH D-2000 High-Performance
98 AF Demagnetizer. The specimens were generally AF-demagnetized in 10–12
99 steps within applied field magnitudes of 3–200 mT. Thermal demagnetiza-
100 tion was carried out using single and dual-chamber paleomagnetic ovens from
101 ASC Scientific. Demagnetization was carried out at ~ 12 heating steps until
102 the maximum unblocking temperature was reached. The magnetic mea-
103 surements were made on an AGICO JR5A spinner magnetometer inside a
104 dynamic Helmholtz cage at Imperial College London.

105 From the pilot studies, AF magnetic cleaning was chosen as the preferred
106 procedure for processing the specimens; from each site, we subsequently sub-
107 jected one additional specimen to thermal demagnetization and seven to
108 AF demagnetization, i.e. a total of ten separately oriented specimens were
109 demagnetized from each site. We analysed the demagnetization data us-
110 ing Puffinplot 1.03beta (Lurcock and Wilson, 2012), and determined the
111 direction of the characteristic remanent magnetization (ChRM) by means
112 of principal component analysis (Kirschvink, 1980). Usually seven or more
113 points were used to determine the line. We corrected the ChRM directions
114 for a small post-emplacement tectonic tilt to the west as defined by dip and
115 azimuth of $\sim 2^\circ$ and $\sim 266^\circ$, respectively (Wensink, 1964b). Site mean direc-
116 tions were calculated using Fisher statistics (Fisher, 1953) and only directions
117 trending to the origin with a maximum angle of deviation (MAD) $< 5^\circ$. Oc-

casional specimen ChRM directions being significant outliers as compared to otherwise well-grouped site directions were discarded for further analysis (see Section S2, Suppl. Mat. for details). Additional specimens from these sites were subjected to AF magnetic cleaning to replace the misbehaved ones. We note that sedimentary samples from sites HNA15 and HNA14 (hyaloclastites) (Figure 2) were excluded in the further analysis because the samples either broke apart during transport or showed non-ideal behaviour to magnetic cleaning.

3.3. *Rock and paleointensity experiment*

As part of our pilot paleointensity experiments we carried out a set of rock magnetic measurements to ascertain the magneto-mineralogy and to assess for possible thermal alteration. The results are presented in Section S3 (Suppl. Mat). We used the IZZI modified protocol (Tauxe and Staudigel, 2004) of the Thellier-Thellier paleointensity experiment (Thellier and Thellier, 1959) to estimate intensity. We initially tested two specimens from all sites for their ability to recover the paleointensity. Based on these and the rock magnetic results, we identified sites suitable for further intensity experiments.

Our first pilot study was carried out on 30 specimens in an applied field of 40 μ T (field applied along the specimens cylindrical axis). This experiment consisted of a series of 28 IZ and ZI heating steps, three pTRM checks and two pTRM tail checks. Samples were generally heated until $\sim 95\%$ of the NRM was demagnetized. The remainder of the pilot studies as well as subsequent intensity experiments were carried out in an applied field of 30 μ T and consisted of series of ~ 34 heating steps, five pTRM checks and four

143 pTRM tail checks. In total, we subjected 205 specimens to IZZI intensity
144 experiments. Due to instrumental problems we had to stop two experiments
145 for four weeks. Subsequent measurements from these experiments were suspi-
146 cious, and measurements related to those specific temperature intervals were
147 deleted before processing the results. All measurements were conducted at
148 Imperial College London.

149 4. Results

150 4.1. $^{40}\text{Ar}/^{39}\text{Ar}$ radiometric dating

151 In order to detect samples still affected by groundmass alteration remain-
152 ing after the acid leaching procedure, 29–35 heating steps were carried out
153 for each sample (Figure 3; Figure S1-1, Suppl. Mat.). The number of low
154 temperature heating steps was increased to ensure an effective removal of any
155 remaining alteration and atmospheric contamination. In 14 or fewer low tem-
156 perature steps, a sufficient amount of discordant gasses were released to allow
157 recognition of horizontal age plateaus with reproducible primary crystalliza-
158 tion ages. Between 11 and 29 of the heating steps define the age plateaus
159 that also include from 43% to 100% of the $^{39}\text{Ar}_\kappa$ gas released. Only one of the
160 eleven groundmasses yielded an age plateau with less than 50% of the total
161 amount of $^{39}\text{Ar}_\kappa$ gas released. Nine out of eleven inverse isochron intercepts
162 are within error of the 295.5 modern atmospheric ratio of $^{40}\text{Ar}/^{36}\text{Ar}$. For
163 all experiments the K/Ca value decreases from the low-temperature steps
164 through the age plateau to the high-temperature steps; most likely a result
165 from alteration phases that readily lose gas at low temperatures while argon
166 retentive phases such as groundmass plagioclase and clinopyroxene tend to

167 degas at high temperatures.

168 Our approach gave high-precision ages (with nominally 1.3–3.8% 2σ un-
169 certainties, including J-value errors), except for sample THA0 that yielded
170 less argon than the rest. TH-14 gave a plateau age of 1.05 ± 0.04 (95.7%
171 $^{39}\text{Ar}_K$) concordant with a total fusion age of 1.02 ± 0.04 Ma, while the in-
172 verse isochron age is 0.73 ± 0.21 Ma. The site polarity (normal) and section
173 magnetostratigraphy suggests an age of 1.05 Ma (Jaramillo) rather than 0.73
174 Ma (Brunhes), and we therefore reject the isochron age for TH-14. Samples
175 KG-2 and HN-13 gave age spectra that suggest modest disturbance with
176 down-stepping ages toward higher temperature steps, likely due to ^{39}Ar re-
177 coil, with superimposed argon loss at low temperature steps. However, the
178 plateau and isochron ages are not different from the total fusion ages at 2σ
179 (Table S1-1, Suppl. Mat.). Regardless of the modest complexities in release
180 behaviour and argon loss, the high-resolution incremental heating age anal-
181 yses on crystalline groundmass samples from Jökuldalur show concordances
182 in plateau, isochron and total fusion ages, indicating that the primary argon
183 reservoirs were not significantly affected by alteration or recoil, and that the
184 K-Ar isotope system has effectively remained closed since the time of erup-
185 tion. For the age model presented in the Discussion we use the plateau ages
186 for all samples except for KG-2 and HN-13 for which we use the total fusion
187 ages (Figure 2).

188 The total age range of the eleven new $^{40}\text{Ar}/^{39}\text{Ar}$ ages (Figures 2, 3)
189 covered by sites TH17 to HN3 is ~ 0.63 – 3.13 Ma. This age range broadly
190 concurs with the chronostratigraphy established by Udagawa et al. (1999)
191 and McDougall and Wensink (1966). However, important deviations occur,

particularly in section KG; the type section for the Gilsá event (Udagawa et al., 1999) (see Discussion).

4.2. Paleodirections

In Figure 4a, we show representative examples of AF and thermal demagnetization data. In general, remanence resides in a stable single component of magnetization acquired during original cooling. A secondary viscous component (VRM) of much smaller magnitude was often removed by AF demagnetization peak fields of 5–15 mT or temperatures of $\sim 200^\circ\text{C}$. In summary, we obtain well-grouped ChRM directions from 49 sites (Table 1), with site mean directions generally being defined by $N > 10$ ($N_{min} = 7$, $N_{max} = 16$), $k > 200$ ($k_{min} = 76$, $k_{max} = 3584$), and $\alpha_{95} < 3.5^\circ$ ($\alpha_{95_{max}} = 5.4^\circ$), where N is the number of independent data at each site, k is the precision parameter, and α_{95} is the circle of 95% confidence (Fisher, 1953). Our re-mapping of Jökuldalur in 2014 indicated that some lava flows were drilled twice. Field observations combined with paleomagnetic results (common mean test) suggest that sites TH16/TH17, KG0/KGA0, HNB15/HNC15, and HN10/HN11, respectively, are units that were drilled twice, i.e. only 45 sites of the 49 sites are distinct. The resulting 10 normal and 35 reverse site mean directions yield Declinations (D) and Inclinations (I) of $D_{normal} = 351.5^\circ$, $I_{normal} = 77.9^\circ$ and $D_{reverse} = 176.8^\circ$, $I_{reverse} = -75.9^\circ$ (Table 1). The normal and reverse directions pass a bootstrap reversals test (Tauxe, 2010) at the 95% level of confidence, having mean directions inside the confidence regions of each other. This allows the data to be combined to an overall combined mean direction for $N = 45$ sites with a result of $D = 355.7^\circ$, $I = 76.3^\circ$, $\alpha_{95} = 3.2$ (Table 1) that is not significantly different from the geocentric axial dipole field for Jökuldalur ($I = 77^\circ$)

217 (Figure 4b).

218 We also calculated the virtual geomagnetic poles (VGPs) for the $N = 45$
219 sites. The VGPs distribute around the North Pole (Figure 4c), and the re-
220 sulting mean paleomagnetic pole ($\bar{\lambda} = 87.8^\circ$, $\bar{\phi} = 224.3^\circ$) is coincident with
221 the North Pole within the 95% confidence limit (Table 1).

222 4.3. Paleointensity

223 The Thellier GUI Auto Interpreter (Shaar and Tauxe, 2013) was used
224 for paleointensity analysis. We visually inspected both the Arai and vector-
225 endpoint diagrams as an initial quality check. For specimens that display
226 relatively linear components of magnetization, the minimum number of suc-
227 cessive points used for the determinations was fixed to $N \geq 10$. In addition,
228 we adopted a relatively strict set of specimen-level cut-off criteria modified
229 after Cromwell et al. (2015, 2013); Selkin and Tauxe (2000): $FRAC > 0.78$,
230 $\beta < 0.1$, $q > 7$ and $DRAT < 10\%$. Our strategy was then to find the set of
231 threshold values for e.g. MAD and DANG that accepted the most sites with
232 $N \geq 3$ successful intensity estimates per site. We found that $MAD < 11^\circ$,
233 $MAD_{anc} < 6^\circ$, $\alpha < 4.8^\circ$ and $DANG < 8.0$ gave good technical results and
234 screened out specimens that we found unreliable.

235 We used all the intensity estimates accepted at each site at the specimen-
236 level to calculate the site median intensity (B) which is less affected by out-
237 liers than the site mean. Given the limited estimates per site ($N = 3 - 9$)
238 we did not filter our results, e.g., by using a certain percentage fraction (or
239 the standard deviation) to set up maximum deviation bounds relative to the
240 site median, and thereby remove what may seem to be outliers. Instead, we
241 report the median intensity for each accepted site along with the minimum

242 and maximum site intensity values.

243 We accepted 44 intensity estimates from 16 sites by the specimen-level
244 cut-off criteria (Table 2: upper part). The *FRAC* used for paleointensity
245 determination ranges from 0.78 to 0.98 with 50% exceeding 0.89, whereas
246 the quality factor q varies from ranges from 7.8 to 27.6 with 50% exceeding
247 12. We regard these as being data of good technical quality.

248 In Figure 5a–e we show representative specimen behaviors for accepted
249 field estimates passing all the specimen-level criteria, including Arai curves
250 that are relatively well-behaved and linear (Figure 5a–c) or nearly linear
251 (Figure 5d–e). Examples of rejected specimens are shown in Figure 5f–h.
252 Figure 5f shows an example of specimens that display linear Arai curves,
253 but fail on the *DRAT* criteria of maximum 10%. Figure 5g shows an ex-
254 ample of distinct concave-up behavior, usually interpreted as characteris-
255 tic of multidomain remanences (Dunlop and Özdemir, 2001). Selecting the
256 low-temperature results in a high-ancient field estimate (61 μT) whereas
257 the high-temperature component results in a low-ancient estimate (12 μT).
258 While both components meet some of the criteria above, they are incompat-
259 ible with each other. In accordance with Cromwell et al. (2013), we rejected
260 specimens with such behaviour until further constraints can be placed on the
261 reliability of concave-up Arai plots. In Figure 5h, we show an example of a
262 specimen with indication of alteration at 250–425°C. The subsequent Arai
263 curve is relatively linear but fails the *FRAC* and *DRAT* criteria. In general,
264 we rejected specimens with such behaviour.

265 Of the 16 sites, only six sites were accepted by the site-level criteria N
266 ≥ 3 (Table 2: lower part). The median paleointensity (\overline{B}) of our six accepted

267 site intensities is $41 \mu\text{T}$ with a median absolute deviation of $3 \mu\text{T}$ (Table 2),
 268 which is less than the present day Iceland field intensity of $\sim 52 \mu\text{T}$. The
 269 minimum and maximum site intensities are $36\frac{37}{34} \mu\text{T}$ (site KG5) and $55\frac{67}{39} \mu\text{T}$
 270 (site THA4), respectively, i.e. only site THA4 gave intensities comparable
 271 to the current intensity. We have added the median intensity estimate (\overline{B}
 272 $= 41 \mu\text{T}$) to the plot in Figure 1a. Our result is within the range of previously
 273 published (non-Holocene; 11 ka – 3.3 Ma) field strength estimates from Ice-
 274 land of $\sim 31 \mu\text{T}$, with minimum and maximum intensities of $12 \mu\text{T}$ and 78
 275 μT , respectively (Cromwell et al., 2015). We also calculated the median vir-
 276 tual axial dipole moment (\overline{VADM}) and the median virtual dipole moment
 277 (\overline{VDM}) for our six intensity estimates (Table 2). We obtain a \overline{VADM} of
 278 57 ZAm^2 with a median absolute deviation of 3 ZAm^2 . The corresponding
 279 latitude-independent \overline{VDM} is $60 \pm 5 \text{ Am}^2$.

280 In Discussion, we compare our high-northern latitude results to high-
 281 southern latitude results from Antarctica (Lawrence et al., 2009), using both
 282 our own cut-off criteria and the less strict specimen-level cut-off criteria of
 283 Lawrence et al. (2009) (see Table S4-1 in Suppl. Mat). Post removal of 11
 284 estimates, considered unreliable, we accepted 84 intensity estimates from 25
 285 sites by the Lawrence et al. (2009) cut-off criteria (see Table S4-2, Suppl.
 286 Mat.). Of these, 14 sites pass our $N \geq 3$ site-level criteria, resulting in
 287 $\overline{B} = 29 \pm 8 \mu\text{T}$, $\overline{VADM} = 40 \pm 11 \text{ ZAm}^2$, and $\overline{VDM} = 42 \pm 12 \text{ Am}^2$. Thus,
 288 eight additional sites were accepted using these criteria, resulting in a lower
 289 median field estimate. However, if looking solely at the six sites accepted
 290 by our preferred criteria (Table 2), \overline{B} increases to $36 \pm 6 \mu\text{T}$ when applying
 291 the criteria of Lawrence et al. (2009), i.e. statistically equal to our preferred

292 estimate of $41 \pm 3 \mu\text{T}$.

293 5. Geomagnetic field behaviour

294 5.1. VGP dispersion and time-averaged inclination

295 A key objective of time-averaged field (TAF) studies is to determine the
296 dispersion of the site mean directions through time (Johnson et al., 2008),
297 which is assumed to be due to paleosecular variation (PSV). The dispersion
298 can be evaluated quantitatively using VGPs from each distinct site (Table 1)
299 and is traditionally represented by the root mean square angular deviation
300 of VGPs about the Earth’s spin axis (Cox, 1969). Here, we used the mod-
301 ified angular standard deviation S_B (Johnson et al., 2008) that corrects for
302 within-site dispersion S_{W_i} .

303 Using all the data from the 45 sites (~ 0.6 – 3.1 Ma interval), taking the
304 antipodes of the reverse poles, we obtain a dispersion $S_B = 19.9^{22.3}_{17.5}$ (95%
305 bootstrap and upper and lower confidence bounds). None of our sites are
306 excluded using a standard VGP latitude cut-off of 45° (e.g., Johnson et al.,
307 2008), therefore the VGP dispersion ($S_{B(45^\circ)}$) using this criterion is the same.
308 According to our revised stratigraphic age model (Section 6), 38 of our sites
309 (TH15 to HN9) are of Matuyama age, one site (TH16/TH17) is of Brunhes
310 age and five (HN8–HN3) are of Gauss age (Figure 2). We calculated a VGP
311 dispersion $S_{B(Mat)} = 20.5^{23.3}_{17.8}$ for our Matuyama age data that is statistically
312 identical to $S_B = 19.9^{22.3}_{17.5}$ obtained for the $N = 45$ data, normal and reverse
313 data combined. Based on the new Jökuldalur data set we cannot exclude
314 differences in dispersion for the Matuyama as compared to the entire ~ 0.6 –
315 3.1 Ma age interval.

316 In order to compare with previous results from Iceland, we calculated S_B
 317 and $S_{B(45^\circ)}$ for (i) the Jökuldalur data set of Udagawa et al. (1999) and (ii)
 318 for a regional Iceland compilation of 1388 site mean VGPs of 0–5 Ma rocks
 319 (see Section S5, Suppl. Mat.). These older data sets are based on surveys
 320 sampling 2–5 cores per site. We also calculated $S_{B(Mat45^\circ)}$ for these data, i.e.
 321 the VGP dispersion for Matuyama age data using a cut-off of 45° . For the
 322 Udagawa data set we obtain $S_B = 23.8 \frac{28.0}{19.9}$ (38 sites), $S_{B(45^\circ)} = 22.1 \frac{25.1}{19.5}$ (37
 323 sites) and $S_{B(Mat45^\circ)} = 21.8 \frac{24.7}{18.9}$ (35 sites), whereas for the regional Iceland
 324 compilation we obtain $S_B = 24.0 \frac{24.7}{23.2}$ (1388 sites), $S_{B(45^\circ)} = 22.5 \frac{23.0}{21.9}$ (1347
 325 sites) and $S_{B(Mat45^\circ)} = 21.4 \frac{22.2}{20.6}$ (688 sites). As evident, the VGP disper-
 326 sion, S_B , $S_{B(45^\circ)}$ and $S_{B(Mat45^\circ)}$, from the older data are $\sim 4^\circ$, $2\text{--}3^\circ$ and $1\text{--}2^\circ$
 327 higher, respectively, than VGP dispersion for the new Jökuldalur data. De-
 328 spite having overlapping 95% levels of confidence the means of S_B for this
 329 study and the study of Udagawa et al. (1999) lie outside the 95% confidence
 330 region of each other and are only just included for $S_{B(45^\circ)}$. For the regional
 331 compilation and the new Jökuldalur data set, the means are not included in
 332 the 95% levels of confidence of each other in any of the calculations. These
 333 results suggest that S_B – and potentially $S_{B(45^\circ)}$ and $S_{B(Mat45^\circ)}$ – are signifi-
 334 cantly lower for the new Jökuldalur data set as compared to the older data.
 335 We speculate that the reduced VGP dispersion is a function of data quality
 336 given the high number of successful ChRMs per site ($N > 10$ on average) for
 337 the new data. Thus, the within-flow scatter of the new data set, as defined
 338 by the α_{95} values (Table 1), show mean and maximum values, respectively,
 339 of 2.7° and 5.4° , with 50% of all α_{95} values being less than 2.7° . These
 340 values are markedly lower than values for the data of Udagawa et al. (1999)

341 ($\alpha 95_{Mean} = 4.1^\circ$, $\alpha 95_{Max} = 7.4^\circ$, 50% of all $\alpha 95$ -values $< 4.0^\circ$) and for the
 342 Iceland compilation ($\alpha 95_{Mean} = 6.0^\circ$, $\alpha 95_{Max} = 23.0^\circ$, 50% of all $\alpha 95$ -values
 343 $< 5.0^\circ$). The above comparisons may stress the importance of maximizing the
 344 number of cores per site, preferably to produce ~ 10 ChRMs per site, and to
 345 maximize the percentage of sun measurements, when carrying out paleomag-
 346 netic surveys in basaltic rocks at high latitudes. This conclusion conforms
 347 with the observations of Johnson et al. (2008) that inclusion of studies with
 348 poor quality data or insufficient samples per site is found to increase S_B .

349 In the following, we focus on the Matuyama which constitutes the main
 350 part of our data set. The geomagnetic field during this reverse polarity chron
 351 is generally regarded as more dispersive and to show stronger dependence of
 352 S_B on latitude as compared to the Brunhes (Johnson et al., 2008); an inter-
 353 pretation that may be evaluated further by adding our high-northern latitude
 354 data. In Figure 6 we plot $S_{B(Mat)}$ for Jökuldalur (this study) together with
 355 $S_{B(Mat45^\circ)}$ values calculated from global Matuyama age data. The data are
 356 plotted against latitude (Jökuldalur at 65°N) together with the expected
 357 VGP dispersion versus latitude for Model G (blue line) of McFadden et al.
 358 (1988) and for the GAD version of the TK03 statistical model (green line)
 359 of Tauxe and Kent (2004). Also shown are the $S_{B(Mat45^\circ)}$ values for the
 360 data of Udagawa et al. (1999) and for the Iceland compilation. As evident
 361 from Figure 6 the VGP dispersion $S_{B(Mat)}$ from Jökuldalur (this study) over-
 362 all supports the interpretation of a dependence of S_B on latitude during the
 363 Matuyama (e.g., Johnson et al., 2008) in the northern hemisphere when com-
 364 pared to other modern-standard data sets, and to predictions from the two
 365 PSV models. Notably, the mean $S_{B(Mat)}$ from our data correlates well with

the trend of Model G of McFadden et al. (1988) but also overlaps with the trend of the TK03 model of Tauxe and Kent (2004) within the 95% confidence levels. Our data therefore show no preference of the two models. We do, however, not observe a clear indication of less dispersive field behavior in the northern hemisphere as compared to the southern hemisphere during the Matuyama as tentatively suggested by Cromwell et al. (2013).

Deviations from a GAD field are often reported as inclination anomalies $\Delta I = I_{obs} - I_{GAD}$, where I_{obs} and I_{GAD} define the observed and predicted (from a GAD field) inclinations (Johnson and McFadden, 2007). A small negative inclination anomaly ($\sim -3^\circ$) was predicted by Johnson et al. (2008) for the Matuyama at 65°N . We obtain a time-averaged inclination anomaly for the 38 Matuyama age data of $\Delta I_{Mat} = -0.91^\circ \frac{2.94}{-4.88}$ (95% confidence limits calculated using a bootstrap technique) that is negligible. In contrast, ΔI_{Mat} for the data of Udagawa et al. (1999) is $-3.42^\circ \frac{0.55}{-7.84}$, i.e. the older data both suggest a higher VGP dispersion and more deviation from a GAD field as compared to the new modern-standard data. The negligible negative inclination anomaly for the Matuyama presented in this study thus provides important high-latitude constraints on the TAF.

5.2. Field strength

Cromwell et al. (2013) presented five field strength estimates from young volcanic rocks (<300 kyr) from Jan Mayen (71°N) located just north of Iceland. They found a high average VADM of 76.8 ± 24.3 ZAm². Recently, Cromwell et al. (2015) added another 44, high-quality, field strength estimates from southern Iceland of which 37 estimates are from rocks younger than 400 kyr, six have an age close to the Matuyama/Gauss boundary and

391 one is of Gauss age. The results of Cromwell et al. (2015) have a median
 392 VADM of 48.6 ± 13.9 ZAm². By comparing their results with field estimates
 393 from Antarctica (Lawrence et al., 2009) over the same time interval, Cromwell
 394 et al. (2015, 2013) argue for the possibility of long-lived hemispheric asym-
 395 metry, contrasting higher fields in the north with lower average strength in
 396 the south. However, this interpretation is hampered by the general lack
 397 of field estimates from the high-latitude southern hemisphere (Figure 1a)
 398 and by the poor temporal overlap of stable field high-latitude intensity re-
 399 sults between the northern and southern hemispheres, in particular for the
 400 Matuyama epoch (Figure 1b).

401 Our new field estimates (Table 2 and Table S4-2) allow us to compare field
 402 strength behavior at relatively high-northern latitudes with field strength es-
 403 timates from Antarctica for the Matuyama. In Figures 7a and 7b we plot 16
 404 recalculated VADMs from Antarctica (Lawrence et al., 2009; Tauxe et al.,
 405 2004b), using a site-level selection criteria of $N \geq 3$ (this study). The Antarc-
 406 tic VADMs are shown together with the paleomagnetic axial dipole moment
 407 model (PADM2M) of Ziegler et al. (2011) for Matuyama down to 2.0 Ma (i.e.
 408 0.78–2.0 Ma); the PADM2M model predicts the geomagnetic field strength
 409 since 2.0 Ma and was derived from both absolute and relative global palaeoin-
 410 tensity data. In Figure 7a we show the six preferred median VADMs from
 411 Jökuldalur (hereafter referred to as Q1-estimates; see Table 2). In Figure 7a
 412 we plot the 11 (0.78–2.0 Ma) VADMs that were produced using the less strict
 413 specimen-level criteria of Lawrence et al. (2009) (hereafter referred to as Q2-
 414 estimates; see Table S4-2, Suppl. Mat.).

415 The median of the PADM2M dipole moment for the period 0.78–2.0 Ma

416 is 49 ± 9 ZAm². This is slightly lower than the median field strength of our six
 417 Q1-estimates of 57 ± 3 ZAm² (Table 2, Figure 7a) but statistically equivalent
 418 to the median field of the 11 (0.78–2.0 Ma) Q2-estimates of 47 ± 9 ZAm². In
 419 contrast, the median VADM of the 16 (0.78–2.0 Ma) field estimates from
 420 Antarctic is only 39 ± 7 ZAm², i.e. significantly lower than our Q1- and Q2-
 421 estimates. Hence, our Matuyama age field strength estimates may support
 422 the hypothesis of higher field strengths in the northern hemisphere on 10^5 – 10^6
 423 time-scales (Cromwell et al., 2015, 2013). However, more paleointensity data
 424 are needed to confirm the inferred asymmetry, in particular from medium
 425 high latitudes at the southern hemisphere and for latitudes $>70^\circ\text{N}$ (Fig-
 426 ure 1a). Interestingly, the very high-field estimates predicted at the southern
 427 hemisphere around 1.36 Ma (106 ZAm²) are partly reproduced for the north-
 428 ern hemisphere data at site THA4 around 1.37 Ma (Q1-estimate = 76 ZAm²;
 429 Q2-estimate = 63 ZAm²), indicating high global field strength.

430 **6. Revised magneto-chronostratigraphy of Jökuldalur**

431 In this section we revise the magneto-chronostratigraphy of Jökuldalur
 432 based on the 11 new $^{40}\text{Ar}/^{39}\text{Ar}$ ages (Figure 2) as well as existing radiomet-
 433 ric ages. In total, 26 K-Ar radiometric ages have been published from sections
 434 TH, KG and HN, indicating an age range of ~ 0.5 – 3.0 Ma (McDougall and
 435 Wensink, 1966; Udagawa et al., 1999; Watkins et al., 1975). Based on paleo-
 436 magnetic and stratigraphic results, we have confidently correlated 19 of these
 437 K-Ar ages to our sites together with two previously published $^{40}\text{Ar}/^{39}\text{Ar}$ ages
 438 (Wijbrans and Langereis, 2003). A full description of the site-to-site corre-
 439 lation and a list of reassigned K-Ar ages are shown in Section S6 (Suppl.

440 Mat.).

441 The K-Ar based magneto-chronostratigraphy of Jökuldalur (McDougall
442 and Wensink, 1966; Udagawa et al., 1999; Watkins et al., 1975) indicates that
443 a significant hiatus of $\sim 400\text{--}500$ kyr is present near the top of section TH.
444 Here, Udagawa et al. (1999) reported an age of ~ 0.5 Ma for site TH16/17,
445 whereas the underlying site TH14 was dated at 0.91 Ma. The results of Uda-
446 gawa et al. (1999) further suggest that (i) the near base of section TH (site
447 TH1; K-Ar age of 1.30 ± 0.06) and the top of section KG (site KG9; K-Ar
448 age of 1.39 ± 0.06) are statistically coeval, (ii) the near base of section KG
449 (site KG0; K-Ar age of 1.85 ± 0.08) is ~ 250 kyr older than site HN16 (K-Ar
450 age of 1.60 ± 0.02) at the top of section HN.

451 The new $^{40}\text{Ar}/^{39}\text{Ar}$ ages of site TH16/17 of 0.63 ± 0.03 Ma and site TH14
452 of 1.05 ± 0.04 Ma (Figure 2) support the interpretation of a major hiatus
453 near the top of section TH although the new ages are ~ 100 kyr older. The
454 new ages of site THA0 (1.51 ± 0.14 Ma) and of TH1 (1.46 ± 0.04 Ma) as
455 well as of site KG9 (1.49 ± 0.03 Ma) are statistically identical and support a
456 small overlap between sections TH and KG (Figure 2). Finally, the new ages
457 of site KG2 (1.88 ± 0.04 Ma; total fusion age) and site HNC15 (1.83 ± 0.04
458 Ma) indicate that some overlap exist between the normal polarity intervals in
459 sections KG and HN. The new age of site HN13 (2.26 ± 0.04 Ma; total fusion
460 age) suggests the normal interval in HN is separated from the underlying
461 reverse interval by a hiatus of ~ 450 kyr, defined by the sedimentary layer of
462 site HNA14.

463 In Figure 8a, we plot the 11 new $^{40}\text{Ar}/^{39}\text{Ar}$ ages together with radiomet-
464 ric ages, confidently correlated to our sites (Table S6-1). All ages are plotted

465 against cumulative stratigraphic height (CSH) of sections TH, KG and HN.
 466 We estimated CSH from the stratigraphic thickness of each site, taking into
 467 account the relative age chronology of the sections (Figure 2) and a regional
 468 tectonic tilt of 2° to the west (Section 2). From Figure 8a it is evident
 469 that several K-Ar ages are up to 200–300 kyr younger than corresponding
 470 $^{40}\text{Ar}/^{39}\text{Ar}$ ages from the same sites (TH17, TH14, TH1, KG9, KG2, HN9) or
 471 from stratigraphically younger sites (TH7, TH8, TH10, KG0), probably in-
 472 dicating variable Ar loss. In contrast, the new and published (Wijbrans and
 473 Langereis, 2003) $^{40}\text{Ar}/^{39}\text{Ar}$ ages for sites HNC15 and HN13 are statistically
 474 identical.

475 In the following, we assume that a segmented linear regression age model
 476 is a valid first order approximation to intervals of ages versus CSH between
 477 inferred hiati, i.e. the volcanic build-up rate is assumed to have remained
 478 fairly constant (cf. McDougall et al., 1977; Watkins and Walker, 1977) for
 479 the period spanned by sections TH, KG and HN. For the linear regression
 480 analysis we used only the $^{40}\text{Ar}/^{39}\text{Ar}$ ages. We initially calculated a linear
 481 regression model for the interval defined by sites KG7 (CSH of ~ 236 m) to
 482 TH15 (CSH of ~ 499 m) (Figure 8b), which contains four new ages and is
 483 bounded above and below by major hiati (Figure 2). Figure 8b shows that
 484 several K-Ar ages (TH5, TH6, TH9, TH12) support the linear regression
 485 model although a majority (e.g., TH1, TH7, TH8, TH11, THA11, KG9) are
 486 significantly younger. Next, we assumed that the KG7-TH15 linear regres-
 487 sion model is a valid approximation for all volcanic stratigraphic intervals of
 488 sections TH, KG and HN. Based on the stratigraphic mapping (Figure 2)
 489 and by using the KG7-TH15 regression model, we defined five main strati-

490 graphic intervals for sections TH, KG and HN; each defined by a linear trend
 491 in age versus CSH and bounded above and below by major hiati (Figure 8b).
 492 We then calculated an interpolated age for all sites (Figure 8c) using the
 493 segmented regression model, and next used this age model to construct a re-
 494 visited magneto-chronstratigraphy for Jökuldalur based on a correlation with
 495 the polarity intervals of GTS2012 (Figure 8d).

496 As evident from Figure 8d sections TH to HN span the Brunhes to Gauss
 497 period, that is, ~ 0.6 – 3.1 Ma. We can confidently correlate the previously
 498 unmapped normal polarity interval, near the top of section TH (Figure 2),
 499 to the Jaramillo subchron at 0.98 – 1.08 Ma, whereas the reverse polarity in-
 500 tervals, HN9–HN13 and HN3–HN8, near the base of section HN probably
 501 belong to Matuyama and a short reverse polarity interval in Gauss around
 502 3.02 – 3.12 Ma, respectively. We note that the reverse polarity site HN4 was
 503 dated at 2.84 ± 0.04 Ma (Figure 8b), i.e. within a Gauss normal polarity
 504 interval. We therefore omitted this age in our regression analysis for the
 505 HN3–HN8 interval.

506 In section HN, the normal polarity interval is defined by sites HNC15–
 507 HN16 (Figure 2). McDougall and Wensink (1966) suggested this interval
 508 contained a single reverse polarity site. Based on K–Ar dating, they cor-
 509 related the lower normal polarity interval to the Olduvai subchron and the
 510 upper interval to a second normal polarity subchron above the older Oldu-
 511 vai subchron. In accordance with the conclusions of Watkins et al. (1975)
 512 we find no evidence of a reverse polarity site within the HNC15–HN16 in-
 513 terval (Table 1; Figure 2). Also, the new $^{40}\text{Ar}/^{39}\text{Ar}$ age of site HNC15 of
 514 1.83 ± 0.04 Ma confirms that the HNC15–HN16 interval belongs to the Oldu-

515 vai subchron (Figure 8d). The underlying ~ 450 kyr long hiatus represented
 516 by the hyaloclastites and brecciated tuffs at HNA14 we correlate with the
 517 thick hyaloclastite deposit at the base of section KG (Figure 2). The hiatus
 518 between sites KG7 and KG6 we correlate with the hyaloclastite below THA0.

519 In section KG, the normal polarity interval is defined by sites KG2–KG6
 520 (Figure 2). This interval was interpreted as the Gilsá event at ~ 1.62 Ma
 521 (Udagawa et al., 1999), based on K-Ar ages of 1.62 ± 0.14 Ma and 1.62 ± 0.06
 522 Ma for sites KG2 and KG4 (Table S6-1). However, Udagawa et al. (1999)
 523 also report a K-Ar age of 1.85 ± 0.08 Ma for the reverse polarity site KG0
 524 (Table S6-1), below their inferred normal Gilsá event. This age is within
 525 the normal polarity Olduvai subchron (Gradstein et al., 2012). Our revised
 526 $^{40}\text{Ar}/^{39}\text{Ar}$ age for site KG2 is 1.88 ± 0.04 Ma (Figure 2), i.e. > 250 kyr
 527 older than the K-Ar age reported by Udagawa et al. (1999). We correlate
 528 the normal interval of sites KG2–KG6 to the Olduvai subchron (Figure 8d),
 529 similar to the HNC15–HN16 interval in section HN (Figure 2). Hence, we
 530 find no evidence of a second normal polarity event around 1.62 Ma (i.e. the
 531 Gilsá event), neither in section KG (Udagawa et al., 1999) nor in section HN
 532 (McDougall and Wensink, 1966).

533 7. Conclusions

- 534 • We present a paleodirectional, paleointensity and magneto-chronostratigraphic
 535 study from Jökuldalur, Iceland. We collected > 700 cores from 51 sites
 536 along three sections.
- 537 • New $^{40}\text{Ar}/^{39}\text{Ar}$ ages are presented from 11 flows. We find that the
 538 drilled lava flows span the age of ~ 0.6 – 3.1 Ma.

- 539 • Based on AF and thermal demagnetization experiments, we obtain
540 well-grouped ChRM directions from 45 distinct sites with site mean
541 directions generally being defined by $N > 10$, $k > 200$ and $\alpha_{95} < 3.5^\circ$.
542 We obtain a mean direction of $D = 355.7^\circ$, $I = 76.3^\circ$, and $\alpha_{95} = 3.2$
543 for the $N = 45$ sites that is not significantly different from a GAD field.
544 Also, the mean paleomagnetic pole ($\bar{\lambda} = 87.8^\circ$, $\bar{\phi} = 224.3^\circ$) is coincident
545 with the North Pole within the 95% confidence limits.
- 546 • We calculate a VGP dispersion $S_{B(Mat)} = 20.5 \frac{23.3}{17.8}$ and an average incli-
547 nation anomaly $\Delta I = -0.91^\circ \frac{2.94}{-4.88}$ for our 38 Matuyama age data. The
548 dispersion S_B overall supports the interpretation of a dependence of
549 S_B on latitude during the Matuyama, while the negligible ΔI suggests
550 little deviation from a GAD field. When comparing to previous results
551 from Jökuldalur and to various Iceland surveys, sampling 2–5 cores per
552 site, the new S_B and ΔI values are lower. We speculate this may be a
553 function of data quality.
- 554 • Based on relatively strict cut-off criteria, we present six field strength
555 estimates from Jökuldalur for the period 1.19–1.83 Ma; a period void
556 of high-northern stable field intensity data. The median field intensity
557 of our six estimates is $41 \pm 3 \mu\text{T}$ (median absolute deviation) with cor-
558 responding VADM and VDM values of $57 \pm 3 \text{ ZAm}^2$ and $60 \pm 5 \text{ Am}^2$. By
559 comparing our results to 16 estimates from Antarctica (VADM of 39 ± 7
560 ZAm^2) for the period 0.78–2.0 Ma, we find support of a higher field
561 strength in the northern hemisphere on 10^5 – 10^6 time-scales. A similar
562 conclusion is reached when using less strict cut-off criteria resulting in

563 14 field estimates from Jökuldalur.

- 564 • Finally, we present a revised magneto-chronostratigraphic model for
565 Jökuldalur. We find no evidence of a second normal polarity event
566 around 1.62 Ma (i.e. the Gilsá event) within the Matuyama.

567 8. Acknowledgements

568 We are grateful to Prof. V. Bachtadse for providing drilling equipment.
569 We also thank Drs. P. Riisager, J. Matzka and L. Kristjannson for assisting
570 the field work planning. The project was funded by the Danish Council for
571 Ind. Res. (12-125623) to A. Døssing. M. S. Riishuus was funded by Rannis
572 and by the Icelandic Centre for Research (09021002). R. Supakulopas was
573 funded from the Dev. and Promotion of Sci. and Tech. Talents Proj.,
574 Thailand.

575 9. References

- 576 Camps, P., Singer, B., Carvallo, C., Goguitchaichvili, A., Fanjat, G., Allen,
577 B., 2011. The Kamikatsura event and the Matuyama–Brunhes reversal
578 recorded in lavas from Tjörnes Peninsula, northern Iceland. *Earth Plane-*
579 *tary Science Letters* 310 (1), 33–44, doi:10.1016/j.epsl.2011.07.026.
- 580 Cox, A., 1969. Confidence limits for the precision parameter κ . *Geo-*
581 *physical Journal International* 17 (5), 545–549, doi:10.1111/j.1365-
582 246X.1969.tb00257.x.
- 583 Cromwell, G., Tauxe, L., Halldórsson, S., 2015. New paleoin-
584 tensity results from rapidly cooled Icelandic lavas: Implications

585 for Arctic geomagnetic field strength. *Journal of Geophysical Re-*
586 *search*, Doi:10.1002/2014JB011828.

587 Cromwell, G., Tauxe, L., Staudigel, H., Constable, C., Koppers, A., Ped-
588 ersen, R.-B., 2013. In search of long-term hemispheric asymmetry in the
589 geomagnetic field: Results from high northern latitudes. *Geochemistry,*
590 *Geophysics, Geosystems* 14 (8), 3234–3249, doi:10.1002/ggge.20174.

591 Dunlop, D. J., Özdemir, Ö., 2001. Beyond Néels theories: thermal demagne-
592 tization of narrow-band partial thermoremanent magnetizations. *Physics*
593 *of the Earth and Planetary Interiors* 126 (1), 43–57, doi:10.1016/S0031-
594 9201(01)00243-6.

595 Fisher, R., 1953. Dispersion on a sphere. *Proceedings of the Royal Society*
596 *of London. Series A. Mathematical and Physical Sciences* 217 (1130), 295–
597 305, doi:10.1098/rspa.1953.0064.

598 Goguitchaichvili, A., Prévot, M., Thompson, J., Roberts, N., 1999. An at-
599 tempt to determine the absolute geomagnetic field intensity in Southwest-
600 ern Iceland during the Gauss–Matuyama reversal. *Physics of the Earth and*
601 *Planetary Interiors* 115 (1), 53–66, doi:10.1016/S0031-9201(99)00064-3.

602 Gradstein, F., Ogg, J., Schmitz, M., Ogg, G., 2012. *The Geologic Time Scale*
603 *2012 2-Volume Set. Vol. 2.* Elsevier.

604 Helgason, J., Duncan, R. A., 2001. Glacial-interglacial history of the
605 Skaftafell region, southeast Iceland, 0–5 ma. *Geology* 29 (2), 179–182,
606 doi:10.1130/0091-7613(2001).

- 607 Hospers, J., 1954. Rock magnetism and polar wandering. *Nature* (173), 1183–
608 1184, doi:10.1038/1731183a0.
- 609 Jicha, B. R., Kristjánsson, L., Brown, M. C., Singer, B. S., Beard, B. L.,
610 Johnson, C. M., 2011. New age for the Skálamælifell excursion and iden-
611 tification of a global geomagnetic event in the late Brunhes chron. *Earth*
612 *Planetary Science Letters* 310 (3), 509–517, doi:10.1016/j.epsl.2011.08.007.
- 613 Johnson, C., Constable, C., Tauxe, L., Barendregt, R., Brown, L., Coe, R.,
614 Layer, P., Mejia, V., Opdyke, N., Singer, B., et al., 2008. Recent investiga-
615 tions of the 0–5 ma geomagnetic field recorded by lava flows. *Geochemistry,*
616 *Geophysics, Geosystems* 9 (4), doi:10.1029/2007GC001696.
- 617 Johnson, C., McFadden, P., 2007. Time-averaged field and paleosecular vari-
618 ation. *Treatise on Geophysics, Geomagnetism Volume*, 417–453.
- 619 Juarez, M., Tauxe, L., Gee, J., Pick, T., 1998. The intensity of the Earth’s
620 magnetic field over the past 160 million years. *Nature* 394 (6696), 878–881,
621 doi:10.1038/29746.
- 622 Kirschvink, J. L., 1980. The least-squares line and plane and the analysis of
623 palaeomagnetic data. *Geophysical Journal International* 62 (3), 699–718,
624 doi:10.1111/j.1365-246X.1980.tb02601.x.
- 625 Kristjánsson, L., 1999. On low-latitude virtual geomagnetic poles in Icelandic
626 basalt lava sequences. *Physics of the Earth and Planetary Interiors* 115 (2),
627 137–145, doi:10.1016/S0031-9201(99)00072-2.

- 628 Kristjánsson, L., Fridleifsson, I., Watkins, N., 1980. Stratigraphy and pa-
 629 leomagnetism of the Esja, Eyrarfjall and Akrafjall mountains, Iceland.
 630 Journal of Geophysics 47, 31–42.
- 631 Kristjánsson, L., Gudmundsson, A., Hardarson, B., 2004. Stratigraphy and
 632 paleomagnetism of a 2.9-km composite lava section in Eyjafjörður, North-
 633 ern Iceland: a reconnaissance study. International Journal of Earth Sci-
 634 ences 93 (4), 582–595, doi:10.1007/s00531-004-0409-4.
- 635 Kuiper, K., Deino, A., Hilgen, F., Krijgsman, W., Renne, P., Wijbrans, J.,
 636 2008. Synchronizing rock clocks of Earth history. Science 320 (5875), 500–
 637 504, doi:10.1126/science.1154339.
- 638 Lawrence, K., Tauxe, L., Staudigel, H., Constable, C., Koppers, A.,
 639 McIntosh, W., Johnson, C., 2009. Paleomagnetic field properties at
 640 high southern latitude. Geochemistry, Geophysics, Geosystems 10 (1),
 641 doi:10.1029/2008GC002072.
- 642 Lurcock, P. C., Wilson, G. S., 2012. Puffinplot: A versatile, user-friendly pro-
 643 gram for paleomagnetic analysis. Geochemistry, Geophysics, Geosystems
 644 13, 10.1029/2012GC004098.
- 645 McDougall, I., Saemundsson, K., Johannesson, H., Watkins, N., Kristjans-
 646 son, L., 1977. Extension of the geomagnetic polarity time scale to 6.5 my:
 647 K-Ar dating, geological and paleomagnetic study of a 3,500-m lava suc-
 648 cession in western Iceland. Geological Society of America Bulletin 88 (1),
 649 1–15, 10.1130/0016-7606(1977)88;1:EOTGPT;2.0.CO;2.

- 650 McDougall, I., Wensink, H., 1966. Paleomagnetism and geochronology of the
651 Pliocene-Pleistocene lavas in Iceland. *Earth and Planetary Science Letters*
652 1 (4), 232–236, doi:10.1016/0012-821X(66)90075-6.
- 653 McFadden, P., Merrill, R., McElhinny, M., 1988. Dipole/quadrupole fam-
654 ily modeling of paleosecular variation. *Journal of Geophysical Research*
655 93 (B10), 11583–11588, doi:10.1029/JB093iB10p11583.
- 656 Opdyke, N. D., Kent, D. V., Huang, K., Foster, D. A., Patel, J., 2010. Equa-
657 torial paleomagnetic time-averaged field results from 0–5 Ma lavas from
658 Kenya and the latitudinal variation of angular dispersion. *Geochemistry,*
659 *Geophysics, Geosystems* 11 (5), doi:10.1029/2009GC002863.
- 660 Panaiotu, C., Visan, M., Tugui, A., Seghedi, I., Panaiotu, A., 2012. Palaeo-
661 magnetism of the South Harghita volcanic rocks of the East Carpathi-
662 ans: implications for tectonic rotations and palaeosecular variation in
663 the past 5 Ma. *Geophysical Journal International* 189 (1), 369–382,
664 doi:10.1111/j.1365-246X.2012.05394.x.
- 665 Selkin, P. A., Tauxe, L., 2000. Long-term variations in palaeointensity. *Philo-*
666 *sophical Transactions of the Royal Society of London A: Mathematical,*
667 *Physical and Engineering Sciences* 358 (1768), 1065–1088.
- 668 Shaar, R., Tauxe, L., 2013. Thellier GUI: An integrated tool for analyzing
669 paleointensity data from Thellier-type experiments. *Geochemistry, Geo-*
670 *physics, Geosystems* 14 (3), 677–692, doi:10.1002/ggge.20062.
- 671 Tanaka, H., Hashimoto, Y., Morita, N., 2012. Palaeointensity determinations

672 from historical and Holocene basalt lavas in Iceland. *Geophysical Journal*
673 *International* 189 (2), 833–845, 10.1111/j.1365-246X.2012.05412.x.

674 Tauxe, L., 2010. *Essentials of paleomagnetism*. University of California Press.

675 Tauxe, L., Gans, P., Mankinen, E. A., 2004a. Paleomagnetism and $^{40}\text{Ar}/^{39}\text{Ar}$
676 ages from volcanics extruded during the Matuyama and Brunhes Chrons
677 near McMurdo Sound, Antarctica. *Geochemistry, Geophysics, Geosystems*
678 5 (6), doi:10.1029/2003GC000656.

679 Tauxe, L., Gee, J., Steiner, M., Staudigel, H., 2013. Paleointensity results
680 from the Jurassic: New constraints from submarine basaltic glasses of
681 ODP Site 801C. *Geochemistry, Geophysics, Geosystems* 14 (10), 4718–
682 4733, doi:10.1002/2013GC004704.

683 Tauxe, L., Kent, D. V., 2004. A simplified statistical model for the geomag-
684 netic field and the detection of shallow bias in paleomagnetic inclinations:
685 was the ancient magnetic field dipolar? *Timescales of the Paleomagnetic*
686 *field*, *Geophysical Monograph Series* 145, 101–115Doi:10.1029/145GM08.

687 Tauxe, L., Lusk, C., Selkin, P., Gans, P., Calvert, A., 2004b. Paleomagnetic
688 results from the Snake River Plain: Contribution to the time-averaged field
689 global database. *Geochemistry, Geophysics, Geosystems* 5 (8).

690 Tauxe, L., Staudigel, H., 2004. Strength of the geomagnetic field in the
691 Cretaceous Normal Superchron: New data from submarine basaltic glass
692 of the Troodos Ophiolite. *Geochemistry, Geophysics, Geosystems* 5 (2),
693 doi:10.1029/2003GC000635.

694 Thellier, E., Thellier, O., 1959. Sur l'intensité du champ magnétique terrestre
695 dans le passé historique et géologique. *Annales de Geophysique* 15, 285–
696 376.

697 Udagawa, S., Kitagawa, H., Gudmundsson, A., Hiroi, O., Koyaguchi, T.,
698 Tanaka, H., Kristjansson, L., Kono, M., 1999. Age and magnetism of
699 lavas in Jökuldalur area, Eastern iceland: Gilsá event revisited. *Physics*
700 *of the Earth and Planetary Interiors* 115 (2), 147–171, doi:10.1016/S0031-
701 9201(99)00073-4.

702 Watkins, N., Walker, G., 1977. Magnetostratigraphy of eastern Iceland.
703 *American Journal of Science* 277 (5), 513–584.

704 Watkins, N. D., Kristjansson, L., McDougall, I., 1975. A detailed paleomag-
705 netic survey of the type location for the Gilsa geomagnetic polarity event.
706 *Earth and Planetary Science Letters* 27 (3), 436–444, doi:10.1016/0012-
707 821X(75)90063-1.

708 Wensink, H., 1964a. Paleomagnetic stratigraphy of younger basalts and inter-
709 calated Plio-Pleistocene tillites in Iceland. *Geologische Rundschau* 54 (1),
710 364–384.

711 Wensink, H., 1964b. Secular variation of earth magnetism in Plio-Pleistocene
712 basalts of eastern Iceland. *Geologie en Mijnbouw* 43, 403–413.

713 Wijbrans, J., Langereis, C., 2003. Elusive Gilsa: Finally laid to rest in north-
714 east Iceland. In: *EGS-AGU-EUG Joint Assembly*. Vol. 1. p. 11595.

715 Ziegler, L., Constable, C., Johnson, C., Tauxe, L., 2011. PADM2M: a pe-
716 nalized maximum likelihood model of the 0–2 Ma palaeomagnetic axial

Table 1: Jökuldalur Paleodirectional Site Statistics

Site	Altitude (m)	SLat (°N)	SLon (°E)	$n_l(n_p)/N$	Dec (°)	Inc (°)	k	α_{95}	VGP Lat	VGP Lon	dp/dm	Polarity	Age (Ma)
TH16	607	65.13987	-15.57405	10/10	305.4	76.2	638.2	1.9	67.2	276.4	3.3/3.5	N	0.56±0.06 ^{°°}
TH17	592	65.13630	-15.57320	10/12	304.6	70	154.4	3.9	61.0	258.8	5.8/6.7	N	0.63±0.03 [°]
TH15	597	65.14237	-15.56368	11/12	156.3	-66.3	217.7	3.1	-69.4	33.3	4.2/5.1	R	
THA15 ^{ns}	582	65.14236	-15.56258	9/18	354.8	69.4	306.8	2.9	77.6	179.2	4.3/5.0	N	
TH14	577	65.14232	-15.56065	8/10	339.7	70.4	1009.5	1.7	75.4	217.7	2.6/3.0	N	1.05±0.04 [°]
TH13	535	65.12205	-15.53512	12/12	149.4	-76.2	336.5	2.4	-76.9	83.2	4.1/4.4	R	
THA13 ^{ns}	534	65.12716	-15.53208	12/14	127.9	-75.9	76.5	5	-68.0	94.2	8.5/9.2	R	
THA12 ^{ns}	534	65.12714	-15.53144	10/14	138.7	-73.7	80.9	5.4	-70.5	77.6	8.7/9.7	R	
TH12	520	65.12938	-15.52793	11/13	198.5	-61.7	265.2	2.8	-65.5	310.4	3.4/4.3	R	
THA11	513	65.12940	-15.52788	11/12	185.4	-54.2	279.7	2.7	-59.5	335.7	2.7/3.8	R	1.18±0.08 ^{°°}
TH11	508	65.12765	-15.52680	10/11	194.4	-61.5	234.2	3.2	-66.1	317.7	3.8/4.9	R	1.10±0.06 ^{°°}
TH10	505	65.12713	-15.52488	10/12	164.2	-71.7	247.3	3.1	-78.5	33.6	4.8/5.4	R	0.91±0.10 ^{°°}
TH9	501	65.12708	-15.52487	8/11	172.7	-73.4	591.4	2.3	-83.2	17.8	3.7/4.1	R	1.19±0.18 ^{°°}
TH8	498	65.12717	-15.52478	10/12	175.4	-78.7	347.8	2.6	-86.4	136.1	4.7/4.9	R	1.02±0.12 ^{°°}
TH7	489	65.12745	-15.52488	10/10	132.3	-79.8	194.8	3.5	-71.7	111.8	6.4/6.6	R	0.98±0.06 ^{°°}
TH6	490	65.12070	-15.51982	11/11	202.3	-68.2	525.4	2	-72.1	294.0	2.8/3.4	R	1.26±0.04 ^{°°}
TH5	467	65.11755	-15.51992	11/11	161.3	-72	225.5	3	-77.9	41.0	4.7/5.4	R	1.26±0.04 ^{°°}
THA4	422	65.11588	-15.51827	12/12	94.9	-86.7	260.5	2.7	-64.9	149.0	5.3/5.4	R	1.22±0.12 ^{°°}
TH4	409	65.11458	-15.51762	10/12	155.6	-85.6	107.9	4.7	-72.8	152.1	9.2/9.3	R	
TH3	415	65.11423	-15.51623	10/16	118.5	-89.2	1404.2	1.3	-65.9	161.0	2.6/2.6	R	
TH2	403	65.11318	-15.51393	10/10	89.3	-86.7	882.1	1.6	-64.2	149.2	3.2/3.2	R	1.26±0.14 ^{°°}
TH1	390	65.11277	-15.51303	12/12	191.8	-77.8	333.3	2.4	-85.0	231.6	4.2/4.5	R	1.46±0.04 [°]
TH0 ^{ns}	349	65.10895	-15.51377	9/9	253.5	-81.2	295.3	3	-64.4	205.7	5.6/5.8	R	
THA0	351	65.10815	-15.51725	11/11	201	-79.2	487.1	2.1	-81.0	218.5	3.8/3.9	R	1.51±0.14 [°]
KG9	507	65.17520	-15.31460	10/10	162.3	-59.1	376.5	2.5	-62.7	15.3	2.78/3.72	R	1.49±0.03 [°]
KG8	505	65.17522	-15.31432	10/10	171.6	-59.7	498.4	2.2	-64.9	359.9	2.46/3.26	R	
KG7	496	65.17485	-15.31370	12/12	160.7	-65.5	320.5	2.4	-69.7	24.6	3.21/3.95	R	
KG6	478	65.17405	-15.31185	9/9	50	84.1	612.7	2.1	70.6	12.6	4.04/4.1	N	
KG5	462	65.17332	-15.31030	9/10	34.6	85.3	218.1	3.5	72.1	2.0	6.85/6.92	N	
KG4	451	65.17300	-15.31008	13/13	353.8	84.5	133.6	3.6	76.0	339.9	7.01/7.1	N	1.62±0.06 ^{°°}
KG3	447	65.17287	-15.30978	11/11	341.4	69.2	215.3	3.1	74.4	210.7	4.52/5.31	N	
KG2	428	65.17223	-15.30902	11/11	21.4	63.3	285.2	2.7	66.5	124.2	3.37/4.27	N	1.97±0.05 [°]
KG1	422	65.17195	-15.30845	10/12	294.9	-75.3	261.2	3	-46.1	202.2	5.01/5.48	R	
KG0	401	65.17073	-15.30758	8/9	171.9	-61.2	214.9	3.8	-66.6	0.0	4.46/5.81	R	1.85±0.08 ^{°°}
KGA0 ^{ns}	372	65.17000	-15.30588	9/10	181.8	-63.9	178.9	3.9	-70.3	341.0	4.88/6.14	R	
HN16	532	65.24460	-15.22970	10/11	333.2	75.2	723.5	1.8	77.9	252.5	3.01/3.29	N	1.60±0.02 ^{°°}
HNB15	497	65.24450	-15.22448	9/11	98.8	88.1	526.6	2.2	64.4	353.5	4.48/4.48	N	
HNC15	482	65.24437	-15.22238	8/10	90	88.2	1058.6	1.7	65.0	353.1	3.4/3.4	N	1.83±0.04 [°]
HN13	458	65.24422	-15.21958	11/12	195	-62.6	635.6	1.8	-67.2	316.0	2.22/2.84	R	2.33±0.06 [°]
HN12 ^{ns}	446	65.24405	-15.21760	10/11	169.4	-72.8	319	2.7	-81.4	25.3	4.29/4.82	R	
HN11	437	65.24392	-15.21622	10/11	209.1	-85.9	707	1.8	-72.0	177.8	3.58/3.61	R	
HN10 ^{ns}	422	65.24368	-15.21540	10/11	213.2	-83.8	449.1	2.3	-74.1	189.9	4.41/4.49	R	
HN9 ^{ns}	406	65.24377	-15.21397	11/11	239.7	-84.4	283.1	2.7	-68.7	192.2	5.28/5.36	R	2.33±0.03 [°]
HN8 ^{ns}	367	65.24336	-15.21147	9/10	207.3	-67.5	2602.1	1	-69.5	288.2	1.4/1.68	R	
HN7 ^{ns}	360	65.24333	-15.21126	10/10	192.1	-67.5	254.1	3	-73.8	316.1	4.22/5.06	R	
HN6	350	65.24335	-15.21074	16/18	208	-79.1	419	1.8	-78.6	223.2	3.26/3.43	R	
HN5 ^{ns}	325	65.24358	-15.20934	7/10	161.5	-79.7	3584.7	1	-81.6	117.0	1.84/1.93	R	
HN4 ^{ns}	309	65.24347	-15.20743	11/12	170.2	-79.8	335.9	2.5	-83.8	132.9	4.56/4.77	R	2.84±0.04 [°]
HN3 ^{ns}	305	65.24334	-15.20719	9(3)/10	135.9	-80	321	2.9	-73.0	112.6	5.4/5.64	R	3.13±0.08 [°]
Mean (all)		65.17	-15.45	45	355.7	76.3	44.8	3.2	87.8	224.3	5.5/5.9		
Normal		65.18	-15.37	10	351.5	77.9	54.6	6.6	86.2	283.5	11.7/12.4		
Reverse		65.17	-15.52	35	176.8	-75.9	42.0	3.8	87.7	203.0	6.5/7.0		

Site: site names of this study ("ns" following the site name denotes sites sampled during cloudy conditions without sun orientations). Altitude: GPS-altitudes in meters. SLat/SLon and Dec/Inc: site latitude/longitude and mean site declination/inclination in geographic coordinates, respectively. n_l : Total number of best-fit lines (including planes, n_p) used in site mean calculations. N: Total number of samples treated from each site. k : Estimate of the Fisher (1953) precision parameter, α_{95} is the Fisher (1953) circle of 95% confidence. VGP Lat/Lon: Virtual geomagnetic poles together with 95% confidence angles in parallel and meridian dp/dm . N/R in the "Polarity" column refer to normal and reverse polarities, respectively. Age[°]: ⁴⁰Ar/³⁹Ar radiometric ages (this study). Age^{°°}: Reassigned K-Ar ages from previous studies (see text). All ages are with 2 σ error. The lower part of the table shows the mean paleodirectional statistics.

Table 2: Statistics for accepted paleointensity results at the specimen-level (upper) and site-level (lower).

Site	Specimen	$T_{min}/T_{max}/n$	FRAC	DRAT	MAD	MAD_{anc}	α	β	q	DANG	B	VADM	VDM
TH17	TH17B2	0/520/14	0.88	9.64	6.04	3.29	2.44	0.07	13.66	3.22	40	56	60
TH10	TH10E2	250/590/15	0.84	2.97	5.56	2.87	1.04	0.05	18.26	1.39	41	57	60
TH10	TH10H2	100/560/14	0.92	9.73	5.44	2.22	1.1	0.03	27.59	1.31	24	33	35
TH10	TH10M2	300/572/12	0.79	7.02	8.71	4.36	1.3	0.05	14.77	1.7	40	56	59
TH10	TH10N1	300/572/12	0.8	5.73	9.65	4.79	1.83	0.09	8.48	2.38	43	60	63
TH9	TH9H1	150/590/15	0.94	3.24	5.86	2.56	0.34	0.03	23.34	0.42	45	62	65
TH8	TH8E2	350/590/13	0.84	5.81	3.79	1.89	0.67	0.06	12.62	0.88	53	74	72
TH8	TH8i1	100/572/16	0.89	8.71	9.42	3.14	1.51	0.05	11.97	1.69	53	74	72
TH7	TH7H2	0/590/18	0.94	4.98	9.18	4.11	1.96	0.04	21.38	2.4	43	60	58
TH7	TH7J1	150/590/15	0.91	6.07	9.74	4.33	3.31	0.07	12.34	3.98	40	56	54
TH7	TH7K2	200/570/14	0.81	3.52	10.24	4.47	2.33	0.05	14.17	2.81	32	44	43
TH7	TH7i1	0/590/18	0.94	4.17	8.87	3.71	0.21	0.04	18.27	0.26	41	57	55
THA4	THA4B2	0/590/19	0.97	5.08	5.99	3.13	1.2	0.04	19.57	1.62	61	85	79
THA4	THA4C1	0/572/17	0.97	6.12	5.46	2.57	0.85	0.07	11.94	1.08	67	93	87
THA4	THA4K1	100/520/12	0.8	9.49	10.36	3.96	0.41	0.06	11.2	0.47	53	74	69
THA4	THA4L2	150/540/12	0.83	9.79	9.44	4.27	2.98	0.08	9.29	3.62	39	54	51
THA4	THA4O1	150/560/12	0.84	8.31	8.44	4.07	3.61	0.06	13.34	4.44	55	76	71
TH2	TH2J1	100/560/15	0.82	4.65	3.23	2.3	1.06	0.1	10.28	1.85	26	36	34
TH1	TH1K2	200/590/16	0.78	3.88	5.77	2.88	2.36	0.08	9.28	2.96	54	75	74
TH1	TH1N1	200/580/14	0.79	6.37	7.67	3.59	1.21	0.09	8.33	1.53	45	62	62
TH1	TH1R2	100/560/15	0.92	8.92	6.17	2.65	2.18	0.05	16.86	2.6	33	46	45
THA0	THA0D2	100/500/12	0.91	3.42	4.46	4.47	4.4	0.04	19.33	7.19	22	31	30
THA0	THA0M1	0/500/13	0.91	9.71	5.96	3.86	4.76	0.04	18.69	6.16	22	31	30
KG8	KG8E2	150/570/15	0.89	9.67	9.21	4.31	3.63	0.04	18.51	4.43	13	18	22
KG5	KG5B2	150/570/13	0.86	0.85	5.74	4	4.15	0.08	9.24	5.76	36	50	47
KG5	KG5D1	0/560/13	0.96	6.49	10.67	5.08	3.11	0.1	9.59	3.88	34	47	44
KG5	KG5F2	150/570/14	0.89	4.88	6.78	3.53	3.48	0.1	8.62	4.36	37	51	48
KG5	KG5H2	0/570/16	0.94	1.99	6.97	3.53	3.69	0.1	9.38	4.55	37	51	48
KG5	KG5i2	0/572/16	0.98	6.26	9.68	4.7	1.99	0.09	10.01	2.54	35	49	46
KG4	KG4I2	0/570/16	0.91	4.03	4	2.13	2.53	0.09	9.84	3.12	34	47	45
KG4	KG4K1	0/560/14	0.89	4.18	4.97	2.93	3.43	0.08	10.4	4.37	34	47	44
KG3	KG3A2	150/570/15	0.87	2.85	6.28	2.95	3	0.07	11.8	3.62	49	68	74
KG3	KG3F2	150/570/14	0.8	6.82	6.19	2.75	2.36	0.07	10.93	2.83	51	71	77
KG3	KG3G1	0/560/15	0.9	7.01	6.37	2.71	3.16	0.09	10.03	3.67	42	58	64
KG3	KG3H2	0/580/16	0.96	10	5.63	2.87	1.67	0.1	9.16	2.17	23	32	35
KG3	KG3I1	0/560/14	0.84	3.02	6.29	2.99	2.34	0.09	10.96	2.88	35	49	53
KG3	KG3L2	300/570/10	0.8	1.26	5.98	3.28	3.54	0.09	7.82	4.46	53	74	80
KG3	KG3M2	150/560/14	0.79	5.59	4.5	1.71	2.04	0.05	14.72	2.3	32	44	49
KG3	KG3N2	0/520/14	0.81	7.25	4.78	1.73	2.17	0.06	10.8	2.42	40	56	61
KG3	KG3O1	100/540/14	0.81	8.46	8.96	3.5	4.41	0.05	13.02	4.99	45	62	68
KG3	KG3P1	0/540/13	0.84	9.85	4.34	1.59	0.96	0.09	7.91	1.1	42	58	64
KG2	KG2R1	0/570/15	0.84	4.9	9.33	2.62	2.96	0.06	8.87	3.18	38	53	62
HN16	HN16K2	0/540/12	0.82	4.62	7.79	4.06	2.37	0.09	9.69	3.11	31	43	44
HN11	HN11G1	100/580/16	0.89	5.52	6.77	2.71	1	0.03	21.85	1.18	58	80	76
Site	SLat (°N)	SLon (°E)	N	Age (Ma)	\bar{B}	B^{upper}	B^{lower}	\bar{VADM}	$VADM^{upper}$	$VADM^{lower}$	\bar{VDM}	VDM^{upper}	VDM^{lower}
TH10	65.12713	-15.52488	4	1.19±0.04*	40	43	24	56	60	33	59	63	35
TH7	65.12745	-15.52488	4	1.22±0.04*	40	43	32	56	60	44	54	58	43
THA4	65.11588	-15.51827	5	1.37±0.04*	55	67	39	76	93	54	71	87	51
TH1	65.11277	-15.51303	3	1.46±0.04	45	54	33	62	75	46	62	74	45
KG5	65.17332	-15.31030	5	1.80±0.03*	36	37	34	50	51	47	47	48	44
KG3	65.17287	-15.30978	9	1.83±0.03*	42	53	23	58	74	32	64	80	35
All sites	65.12857	-15.45429	6	~1.19–1.83	41±3			57±3			60±5		

N: Number of specimens used to calculate site median intensity after meeting the specimen-level cut-off criteria listed in Section 4.3 and the $N \geq 3$ site-level criteria. B : Field strength (μT). VADM: Virtual axial dipole moment (ZAm^2). VDM: Virtual dipole moment (Am^2). \bar{B} , \bar{VADM} and \bar{VDM} are median values given with median absolute deviation. Age for site THA0 is new Ar-Ar ages (this study). Ages marked with * are interpolated model ages based on 1st order segmented regression analysis of new and published Ar-Ar ages (see text).

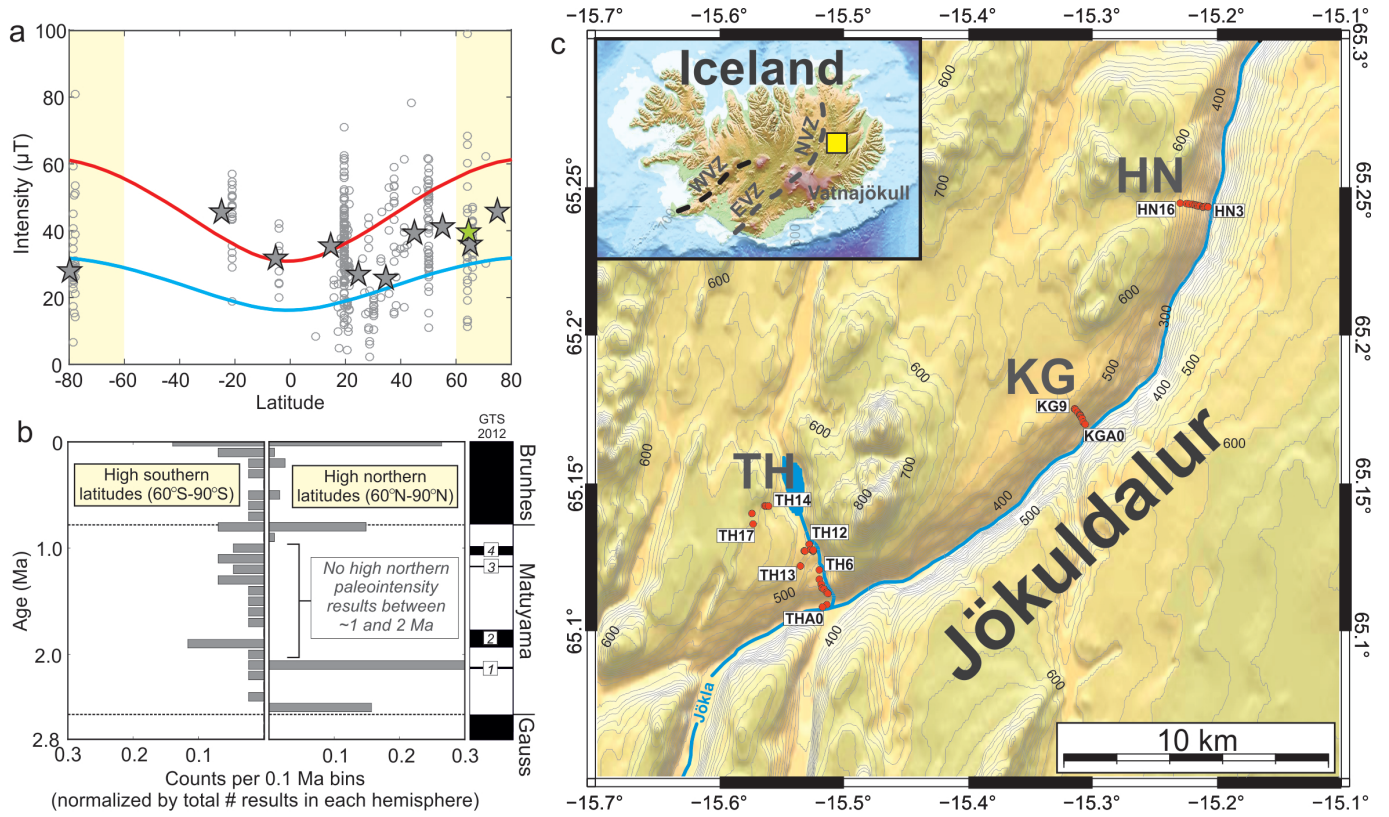


Figure 1: (a) Site-level paleointensity data (0–5 Ma) passing $N \geq 3$ site-level criteria (downloaded from the PINT database at <http://earth.liv.ac.uk/pint/>). Data are plotted against latitude, and median values for 10° bins are shown as grey stars. Green star: Median paleointensity obtained from Jökuldalur (this study; $41 \mu\text{T}$). Predicted values for the present dipole moments of 80 ZAm^2 is shown as red line and for the long-term average field of 42 ZAm^2 ((5–160 Ma, Juarez et al., 1998) and (0–140 Ma, Tauxe et al., 2013)) as blue line. (b) Summary histograms of published field strength estimates. Notice the lack of high-northern data between 1 and 2 Ma. (c) Topographic map of Jökuldalur. Red dots: Location of drill sites (this study) along sections TH (Thverá), KG (Krengilsá) and HN (Hnjúksá). Inset: Topographic map of Iceland. Black dotted lines show location of the main volcanic rift zones. Yellow box: Outline of the area in the main map. Abbreviations: EVZ, Eastern Volcanic Zone; NVZ, Northern Volcanic Zone; WVZ, Western Volcanic Zone.

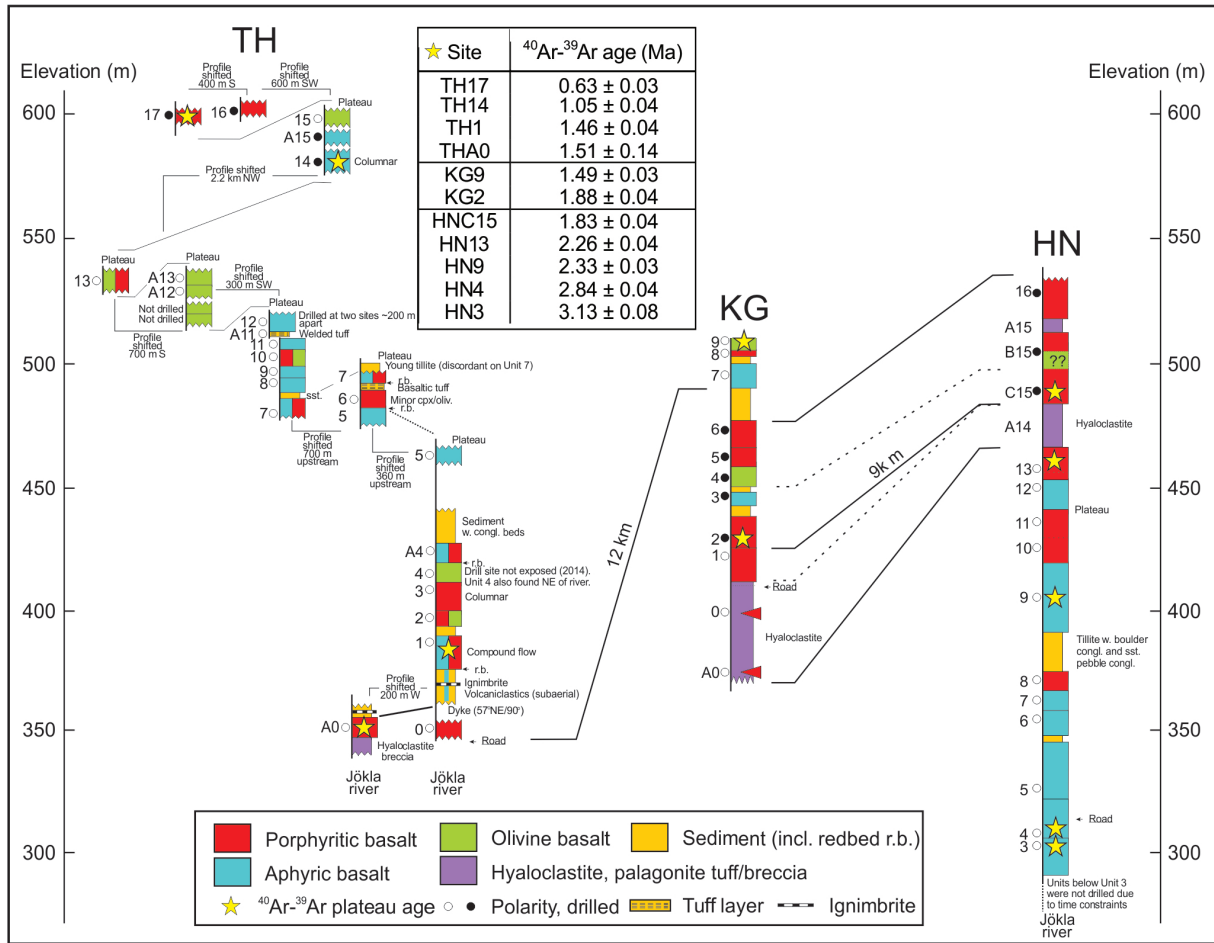


Figure 2: Updated stratigraphy of sections TH, KG and HN. For location, see Figure 1c. Labels to the left are site labels (this study). White(black) filled circles are magnetic reverse(normal) polarity. Yellow stars: New $^{40}\text{Ar}/^{39}\text{Ar}$ ages (this study). The ages for KG2 and HN13 are total fusion ages (see text). Note the normal polarity intervals in sections KG and HN. The normal polarity interval in section KG was interpreted as the Gilsá event by Udagawa et al. (1999). We correlate both the normal polarity intervals in sections KG and HN to the Olduvai subchron (see text).

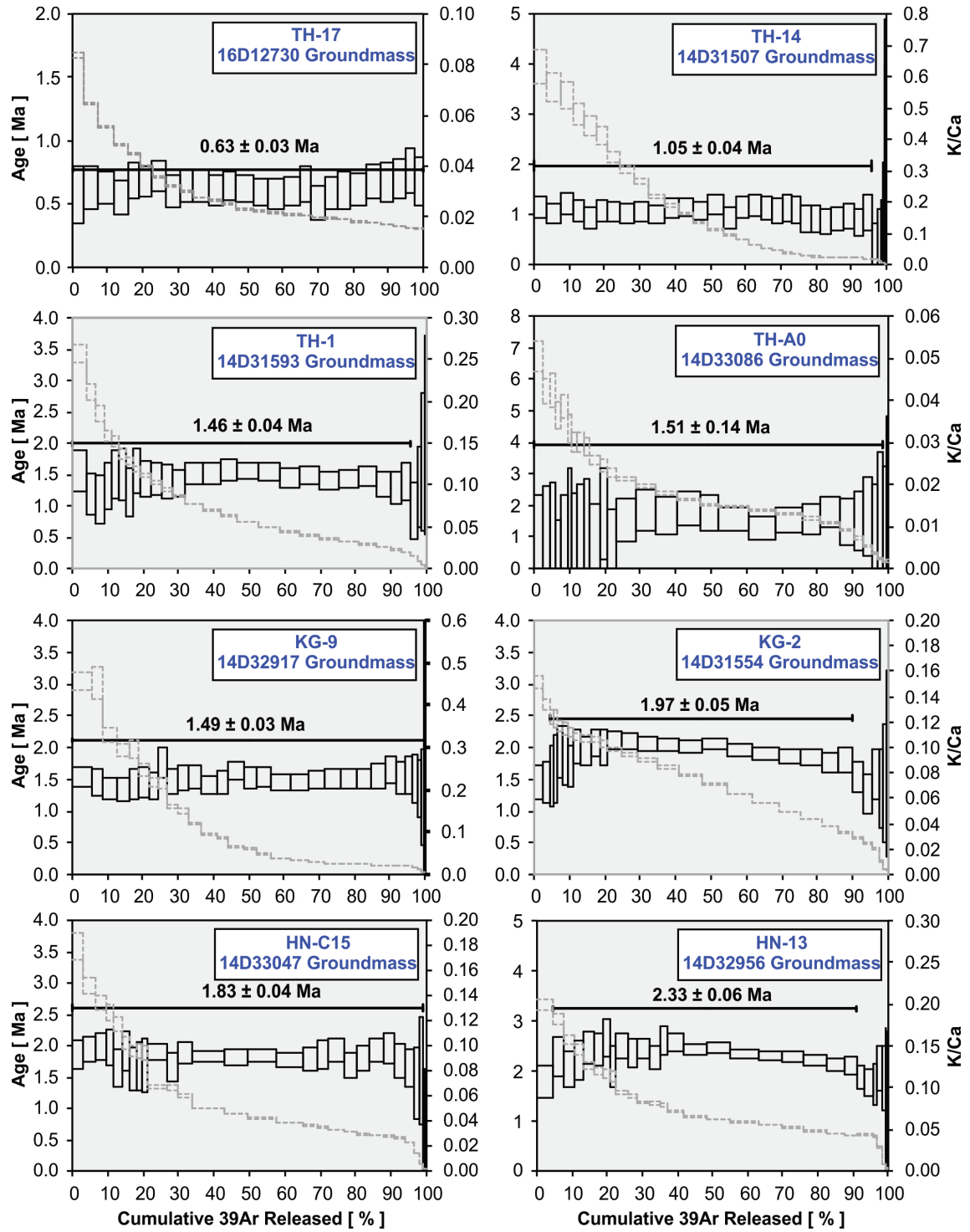


Figure 3: High-resolution incremental heating $^{40}\text{Ar}/^{39}\text{Ar}$ age spectra on groundmass separates of subaerial basalt samples from profiles TH, KG and HN. The age spectra are presented in stratigraphic order from young to old in the lava pile. The $^{40}\text{Ar}/^{39}\text{Ar}$ ages are weighted age estimates with errors reported at the 95% confidence level, including 0.2-0.3% standard deviations in the J-value. All samples were monitored against FCT sanidine (28.201 ± 0.023 Ma, 1σ) as calibrated by Kuiper et al. (2008). Solid black lines are $^{40}\text{Ar}/^{39}\text{Ar}$ ages and stippled gray lines are K/Ca values. Data are listed in Table S1-1 (Suppl. Mat.).

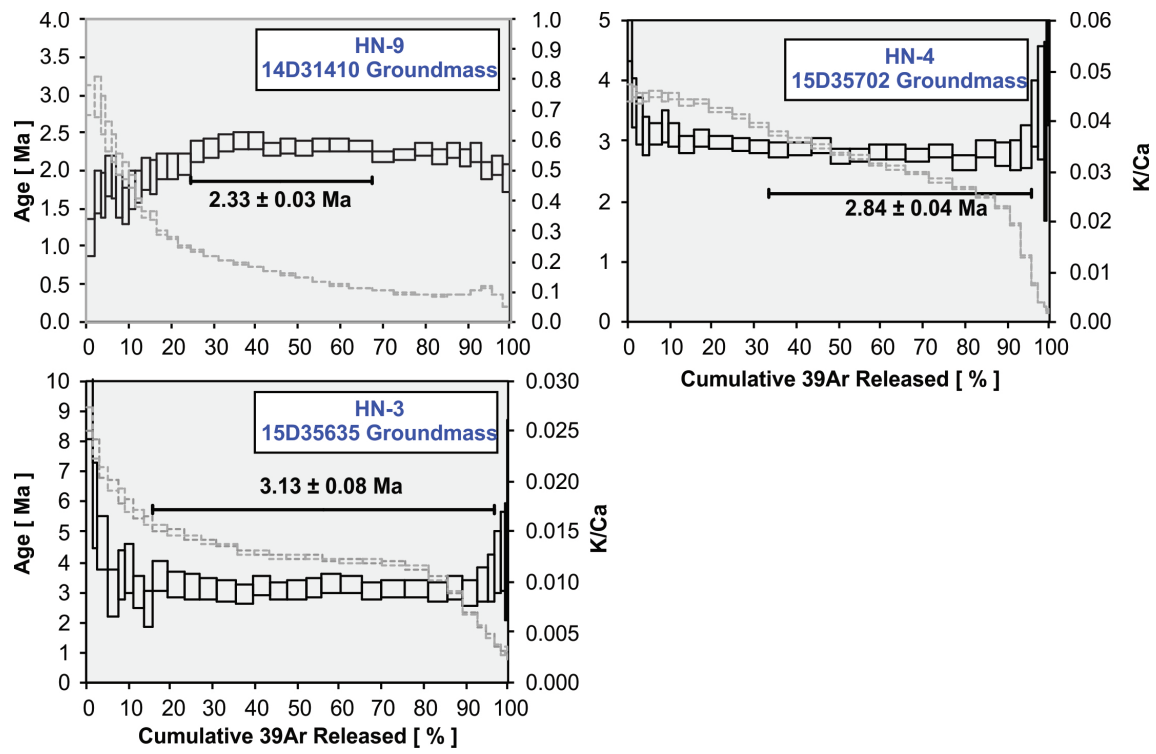


Figure 3: Continued

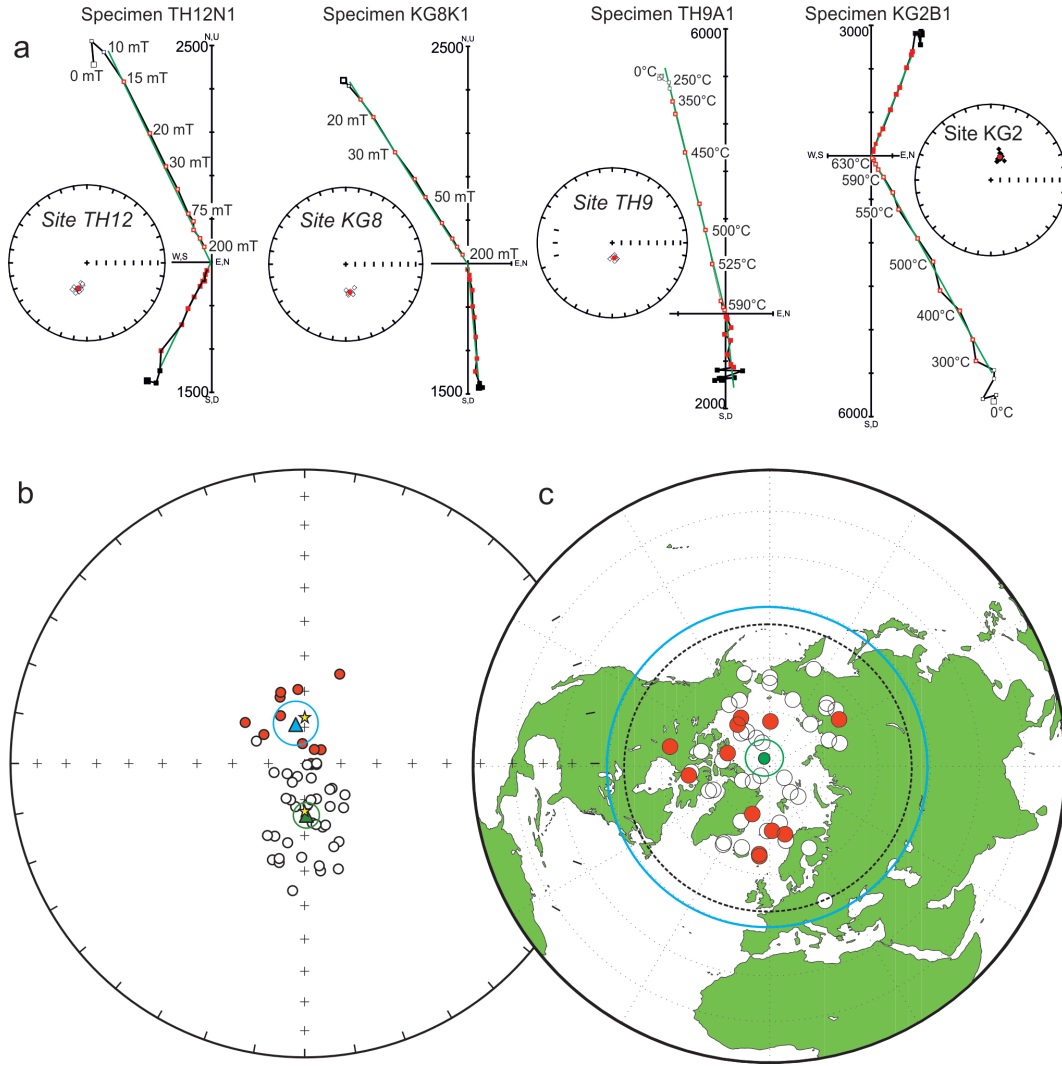


Figure 4: (a) Representative Zijderveld diagrams of AF (alternating-field) and thermal demagnetization experiments. Values along axes are magnetization (mA/m). Closed(open) circles are the horizontal(vertical) plane projection of the directional vector. Inset figures: Site mean directions for the corresponding sites. Red squares mark the site means. (b) Equal area projection of site-mean directions for Jökuldalur. Filled (open) circles plot on the lower (upper) hemisphere. Grand mean directions (triangles) with $\alpha 95$ confidence cones for normal (blue circle) and reversed (green circle) sites. Yellow stars: Expected directions from a GAD field. (c) VGP positions for all sites. Dotted black circle is at 50.2° latitude (Vandamme). Full blue circle is at 45° latitude. Filled (open) circles are northern hemisphere (antipodes of southern hemisphere) VGP positions. Filled green circle: grand mean VGP (paleomagnetic pole) for the 45 distinct sites with 95% confidence cone that encompasses the North Pole.

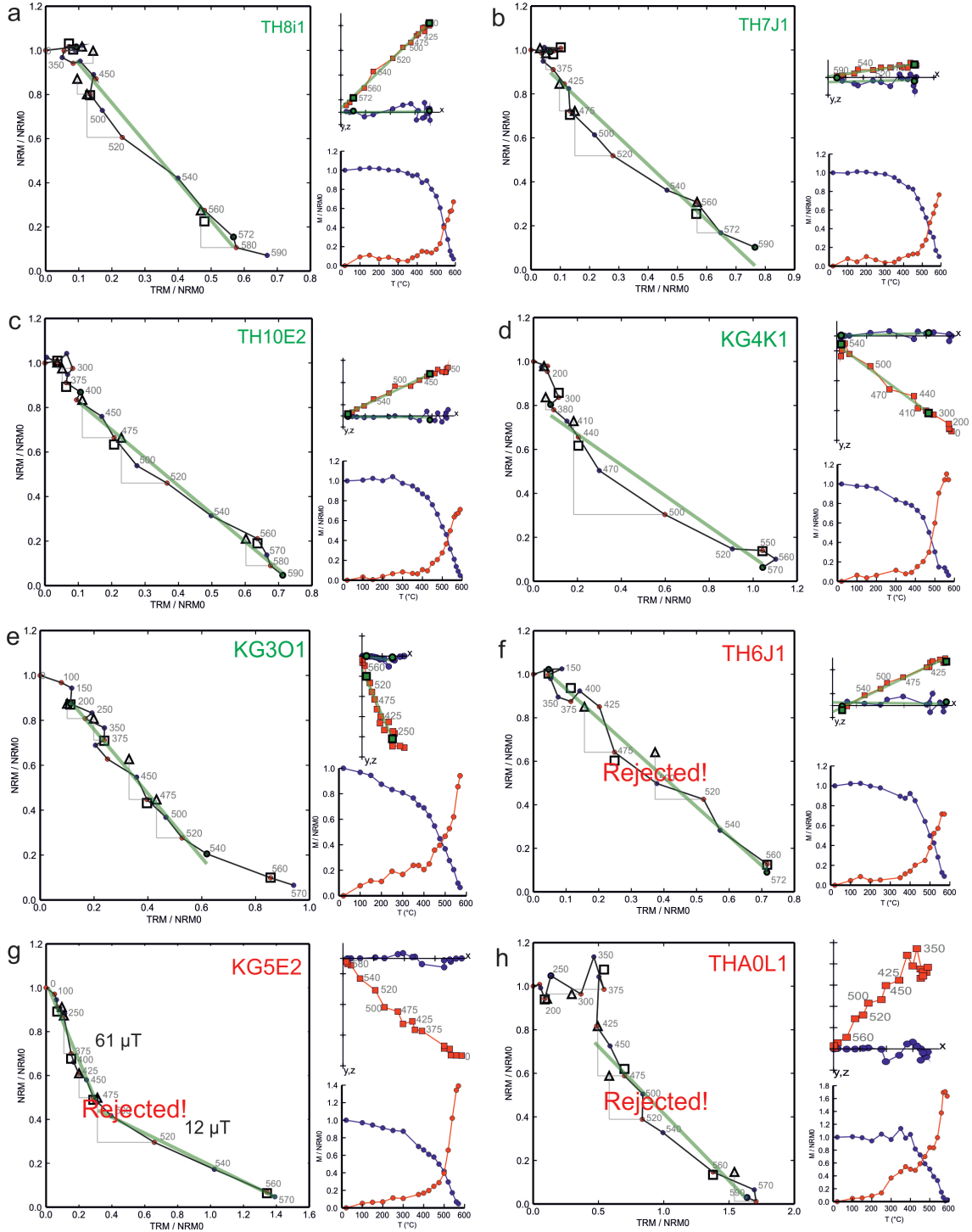


Figure 5: Representative paleointensity results displayed by Arai plots, vector end-point diagrams and NRM-decay/TRM-growth curves for each specimen. (a)–(e) Accepted and (f)–(h) Rejected specimen examples using our preferred cut-off criteria listed in Section 4.3. In (g): Two paleointensity estimates are shown (high and low temperature components); each of which could be valid under certain selection criteria. For our preferred intensity estimates in Table 2 (Q1-estimates; see text) we rejected specimens showing such behavior. pTRM checks are shown as open triangles, pTRM tail-checks as open squares, zero-field/in-field (ZI) temperature steps shown as red dots and IZ steps shown in blue. The green line is the least-squares component for selected temperature steps generated by Thellier GUI Auto Interpreter (Shaar and Tauxe, 2013). Vector end-point diagrams are x-y (x-z) projections of the NRMs in the specimen coordinate system, where x axis is rotated to the direction of the NRM in the x-y plane. NRM-decay curves are shown in blue, TRM-acquisition curves in red.

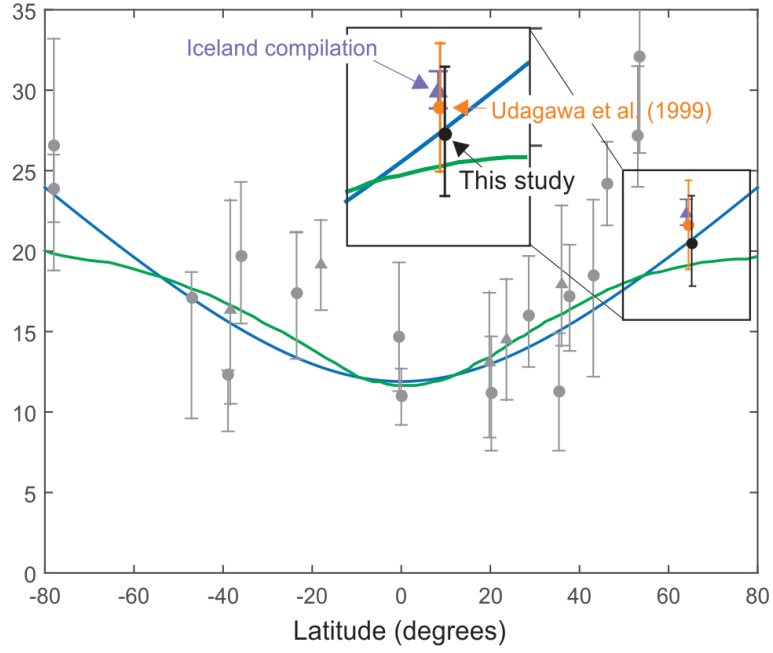


Figure 6: VGP dispersion as a function of latitude for Matuyama age data (0.78–2.58 Ma). Inset: Zoom-in of Jökuldalur results (this study and Udagawa et al. (1999)) and dispersion for a regional Iceland compilation (see Table S5-1, Suppl. Mat.). Mean dispersion from Jökuldalur (this study) shown as black. Mean dispersion from Jökuldalur (Udagawa et al., 1999) shown as orange. Mean dispersion from the Iceland compilation shown as purple. Mean dispersion from various global studies (Cromwell et al., 2013; Johnson et al., 2008; Lawrence et al., 2009; Opdyke et al., 2010; Panaiotu et al., 2012) shown in filled grey circles and regional compilations (cf. Johnson et al., 2008) in filled grey triangles. Errors bars are 2σ . All data have $k > 50$, and latitude cutoff of 45° . Blue line: Model G (McFadden et al., 1988). Green line: TK03 (Tauxe and Kent, 2004).

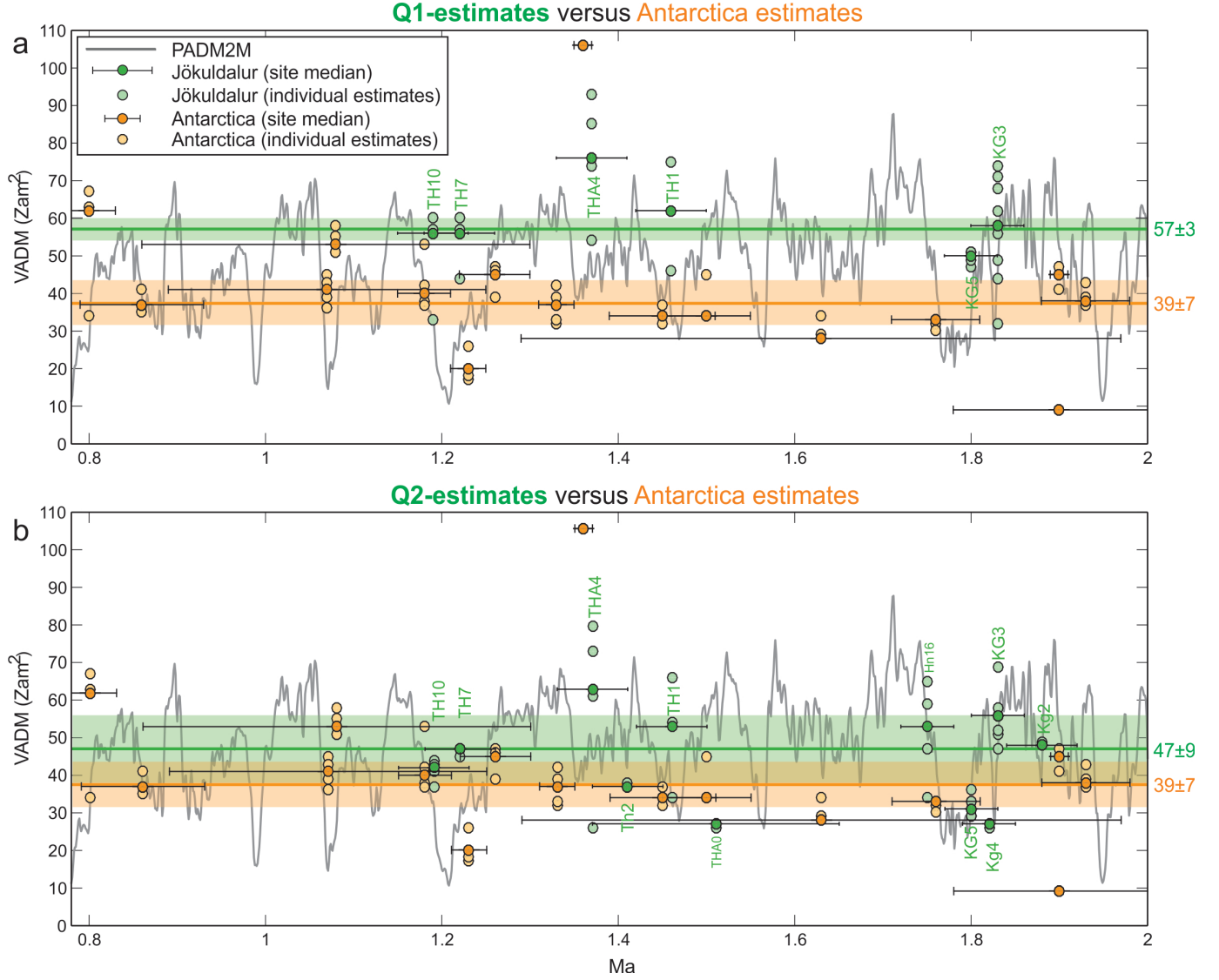


Figure 7: Virtual axial dipole moments (VADMs) versus time for the interval 0.78–2 Ma. Grey line: PADM2M time-varying paleomagnetic axial dipole moment model (Ziegler et al., 2011). Dark(light) filled green circles: Site-level median (dark) and individual (light) field strengths from Jökuldalur (this study). The ages of the Jökuldalur data are based on new Ar-Ar ages and from interpolated model ages (Section 6). All ages given with errorbars of 2σ . Dark(light) filled orange circles: 16 site-level median (dark) and individual (light) field strengths from Antarctica (Lawrence et al., 2009) that satisfy a site-level cut-off of $N \geq 3$. (a) Preferred field strength estimates (Q1) from Jökuldalur (see Table 2). (b) Alternative field estimates (Q2) from Jökuldalur using the less strict specimen-level criteria of Lawrence et al. (2009) and a site-level cut-off of $N \geq 3$ (see Table S4-2, Suppl. Mat.). We note that a higher median field is observed for the high-northern Q1 and Q2 data (green horizontal lines) as compared to the high-southern data (orange horizontal line). The horizontal lines are plotted with transparent horizontal bars according to their median absolute deviation.

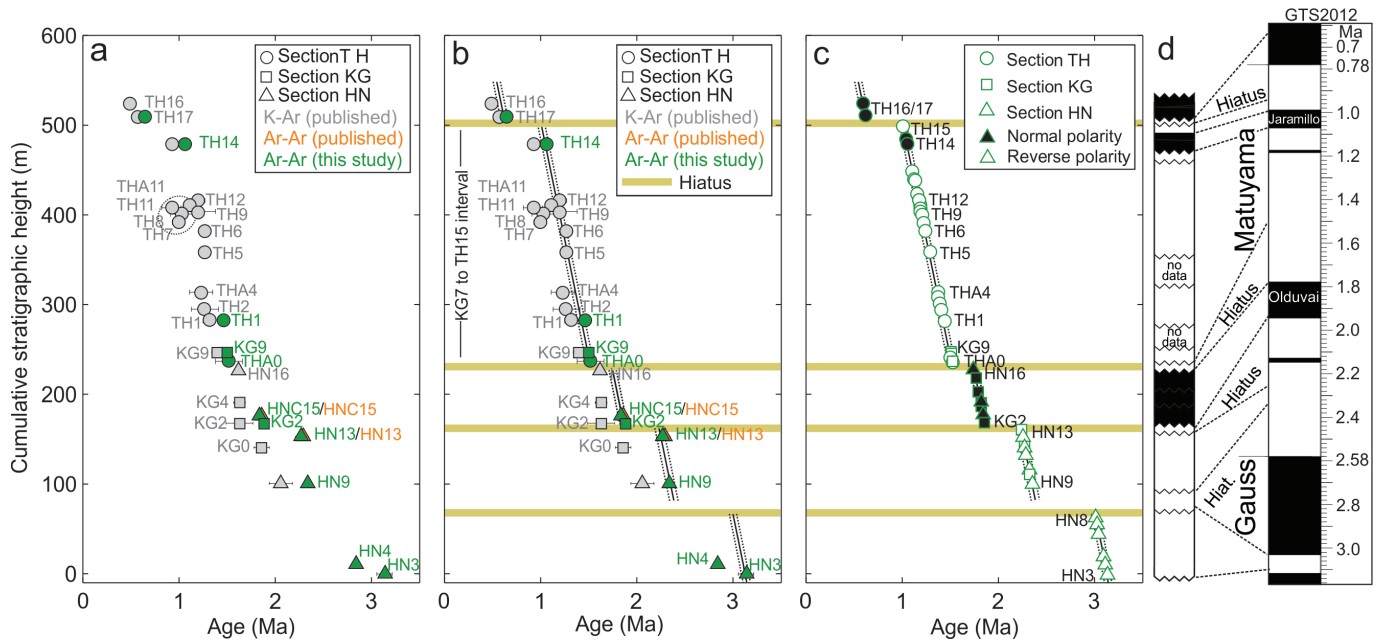


Figure 8: (a) K-Ar and Ar-Ar ages versus cumulative stratigraphic height (CSH) for sections TH, KG and HN in Jökuldalur. Published radiometric K-Ar and Ar-Ar ages are taken from Watkins et al. (1975), Udagawa et al. (1999) and Wijbrans and Langereis (2003), respectively. Only published ages from sites that can we confidently correlate to our sites are shown (cf. Table S6-1, Suppl. Mat.). New Ar-Ar ages are from this study. (b) 1st order segmented regression model based on Ar-Ar data only. The regression model (thin black lines) is shown with 2 σ error (thin dotted lines). Also shown are major hiati in the stratigraphic column. (c) Interpolated (model) ages for all sites according to their CSH. Black(white) symbols are normal(reverse) polarity. (d) Revised magneto-chronostratigraphic model for sections TH, KG and HN based on correlation to GTS2012 (Gradstein et al., 2012). We find no evidence for the Gilsá event in sections KG or HN, where both normal polarity intervals can be correlated to the Olduvai subchron. We do, however, suggest that the short Jaramillo subchron is present near the top of section TH.